THE JOURNAL OF BIOLOGICAL CHEMISTRY VOL. 289, NO. 17, pp. 11952–11969, April 25, 2014


# T-type Channels Become Highly Permeable to Sodium Ions Using an Alternative Extracellular Turret Region (S5-P) Outside the Selectivity Filter*◆

Received for publication, January 22, 2014, and in revised form, February 28, 2014 Published, JBC Papers in Press, March 4, 2014, DOI 10.1074/jbc.M114.551473

**Adriano Senatore**[1,2], **Wendy Guan**[1], **Adrienne N. Boone, and J. David Spafford**[3]

*From the Department of Biology, University of Waterloo, Waterloo, Ontario N2L 3G1, Canada*

**Background:** Ion selectivity of voltage-gated channels is governed by selectivity filters.
**Results:** Alternative turret region in domain II promotes highly sodium-permeable T-type channels without major changes to gating and kinetic features.
**Conclusion:** T-type channels can generate variable sodium or calcium permeability by gene splicing.
**Significance:** Ion selectivity in T-type channels can be altered using extracellular domains outside the ion selectivity filter.

**T-type ($Ca_v3$) channels are categorized as calcium channels, but invertebrate ones can be highly sodium-selective channels. We illustrate that the snail $LCa_v3$ T-type channel becomes highly sodium-permeable through exon splicing of an extracellular turret and descending helix in domain II of the four-domain $Ca_v3$ channel. Highly sodium-permeable T-type channels are generated without altering the invariant ring of charged residues in the selectivity filter that governs calcium selectivity in calcium channels. The highly sodium-permeant T-type channel expresses in the brain and is the only splice isoform expressed in the snail heart. This unique splicing of turret residues offers T-type channels a capacity to serve as a pacemaking sodium current in the primitive heart and brain in lieu of $Na_v1$-type sodium channels and to substitute for voltage-gated sodium channels lacking in many invertebrates. T-type channels would also contribute substantially to sodium leak conductances at rest in invertebrates because of their large window currents.**

$Ca_v3$ T-type channels are members of the 4×6TM (4 heterologous domains of 6 transmembrane segments) family of voltage-gated ion channels, which includes calcium ($Ca_v$) and sodium ($Na_v$) channels and sodium leak conductance channel (NALCN) (1–3). The four heterologous domains of 4×6TM channels are considered to have evolved from two rounds of duplication of ancestral channels with one domain, such as the voltage-gated potassium channels (4). Key elements of each domain are a voltage sensor region (segments 1–4) and a re-entrant pore loop that extends from segments 5 and 6 and contains the selectivity filter thought to govern ion selectivity. The potassium channel pore mimics the hydration shell oxygen atoms that surround potassium ions in solution using conserved selectivity filter residues consisting of backbone carbonyl oxygens (5). This configuration makes it energetically feasible for surrogate oxygen groups to displace hydrating water molecules as potassium ions permeate (5). P-(Pore-) loops are contributed by four asymmetrical domains of calcium and sodium channels to a wider and shorter selectivity filter, which allows sodium ions to pass in a semi-hydrated (6) or hydrated state (7). Side chains of glutamate residues (EEEE) in the selectivity filter project carboxyl oxygens into the pore to create a high affinity pore locus for calcium ions in $Ca_v1$ (L-type) and $Ca_v2$ (non-L-type) calcium channels (8), where $Na^+$ ions are prohibited from passing in the presence of low concentrations of external $Ca^{2+}$ ions (~1 $\mu$M) (9). T-type channels ubiquitously have a similar negatively charged ring of residues as $Ca_v1$ and $Ca_v2$ channels in the selectivity filter, but they are notably different, with aspartate residues replacing two of the glutamate residues in the 3rd and 4th positions (EEDD). Mammalian T-type channels ($Ca_v3.1$, $Ca_v3.2$, and $Ca_v3.3$) have an ~10-fold lower calcium selectivity over sodium than $Ca_v1$ and $Ca_v2$ channels, but they are still impermeant to sodium in the presence of low (10 $\mu$M) calcium (10, 11). Here, we show that the $LCa_v3$ T-type channel from the pond snail *Lymnaea stagnalis* with a standard EEDD selectivity filter becomes highly permeant to monovalent cations through splicing of a novel extracellular turret, even in the presence of physiological (millimolar) concentrations of $Ca^{2+}$ ions. These sodium-permeant T-type currents serve as a major pacemaker current of primitive hearts, and are likely proxy for sodium channels when they are absent in many invertebrates. Our work confirms the capacity of snail channel currents to switch sodium and calcium permeabilities by an extracellular determinant, first postulated by Kostyuk *et al.* (12) more than 30 years ago.

## EXPERIMENTAL PROCEDURES

*Cloning and Expression of Novel $LCa_v3$ Exon 12a Splice Variant*—The original cloning and expression work of $LCa_v3$ T-type calcium channel containing exons +8b, 12b, and −25c was described in Senatore and Spafford (13), and the original

* This work was supported in part by a Heart and Stroke Foundation of Canada grant-in-aid and Natural Sciences and Engineering Research Council of Canada discovery grant (to J. D. S.).
◆ This article was selected as a Paper of the Week.
*The nucleotide sequence(s) reported in this paper has been submitted to the GenBank™/EBI Data Bank with accession number(s) JX292155.*
[1] Both authors contributed equally to this work.
[2] Supported by Natural Sciences and Engineering Research Council of Canada Graduate Scholarship and Ontario Graduate Scholarship award.
[3] To whom correspondence should be addressed: B1-173, Dept. of Biology, University of Waterloo, Waterloo, Ontario N2L 3G1, Canada. Tel.: 519-888-4567 (Ext. 38186); Fax: 519-746-0614; E-mail: spafford@uwaterloo.ca.

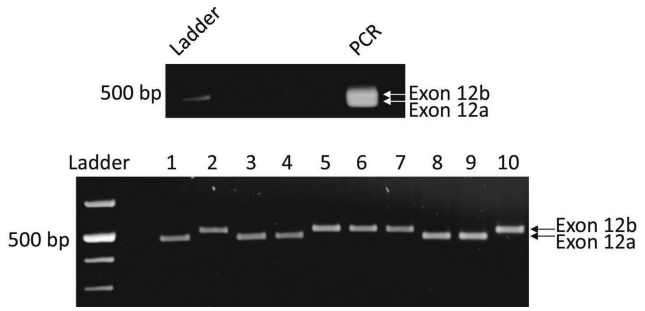


FIGURE 1. **Expression of exons 12a and 12b in *L. stagnalis* cDNA.** *Top,* PCR amplification of snail embryonic cDNA with nested primers flanking the mutually exclusive exons 12a and 12b produced two DNA fragments that could be distinguished in size on an agarose gel. *Bottom,* plasmid DNA inserts from *A* were excised from the pGEM-T Easy vector with EcoRI, and electrophoresed inserts were restricted to two sizes (451 bp for exon 12a and 484 bp for exon 12b, plus additional sizes for polylinker sequence from the pGEM vector). Sequencing of multiple inserts of each size confirmed that the smaller plasmid insert encoded exon 12a and the larger clone encoded exon 12b.

gene sequence was deposited as GenBank™ accession number AF484084. Subsequently, we described $LCa_v3$ T-type calcium channel splicing of exon 8b deposited as GenBank™ accession number JQ313138 and exon 25c deposited as GenBank™ accession number JQ313139. $LCa_v3$ −8b and +25C splice variants were described in Senatore and Spafford (14). Here, we describe novel exon 12a isoform (+8b, 12a, −25C), created by PCR using the original full-length clone of $LCa_v3$ in pIRES2 vector (+8b, 12b, −25c) as template. The novel splice variant (+8b, 12a, −25C) has been deposited as GenBank™ accession number JX292155. The inclusion of exons +8b (54%) and 12a (56%) and −25C (77%) is the most common configuration of these three exons in the adult brain, whereas the adult heart does not commonly have a configuration of +8b (16%) or −25C (21%) (14). The adult heart configuration of exons most commonly found is −8b (84%), 12a (99%), and +25C (79%) (14). Novel exon 12a was confirmed in multiple PCR amplifications from snail brain cDNA (Fig. 1). All expressed plasmids were confirmed by sequencing (TCAG DNA Sequencing Facility, Sick Kids Hospital, Toronto, Canada). Human $Ca_v3.1$ expressible clone was a gift from Gerald Zamponi, University of Calgary, and cloned by Aaron Beedle.

*Culturing of Snail Heart Cells*—Heart ventricle cells were cultured from anesthetized adult snails (25–35 mm shell length) using a modified protocol (15). Cut up ventricles were placed in 0.5 mM $Ca^{2+}$ Leibowitz medium containing gentamycin (400 mg/ml) and 30 mM glucose, trypsinized (0.25% (w/v) trypsin, Sigma T9201) for 10 min, and then treated with 0.1% collagenase (Sigma type II) in 0.5 mM $Ca^{2+}$ Leibowitz medium for 30 min. The digested hearts were then washed three times with 3.5 mM $Ca^{2+}$ Leibowitz medium and then plated on acid-etched circular glass coverslips (16) and left for 24 h to adhere at room temperature in 3.5 mM $Ca^{2+}$ Leibowitz medium containing 400 mg/ml gentamycin, 30 mM glucose, and 2% fetal bovine serum, before patch clamp recording 24 h later.

*Whole Cell Patch Clamp Recording*—We have detailed our optimized technique for the culture and maintenance of mammalian HEK-293T cells, calcium phosphate transfection and expression of ion channels, and their recording using whole cell patch clamp in an on-line video journal (17). There are five sets of solutions for recording (Tables 1 and 2). For comparing ion permeabilities or drug block, a Valvelink8.2® gravity flow Teflon perfusion system (AutoMate Scientific, Berkeley, CA) was used to toggle between differing external solutions during electrophysiological recording. Mibefradil was diluted in 5 mM water. A stock solution of isradipine was made in DMSO (dimethyl sulfoxide). Final concentration of isradipine was in 0.01% DMSO.

Whole cell patch clamp recordings were carried out with an AxoPatch 200B amplifier, combined with a Digidata® 1440A data acquisition system and pCLAMP 10 software. Patch pipettes for recording had pipette resistances of 2–5 MΩ (HEK-293T cells) or 5–10 MΩ (heart cells) and with typical access resistance maintained after breakthrough between 4 and 6 MΩ (HEK-293T cells)

**TABLE 1**
External and internal recording solutions (part 1)

**$[Ca^{2+}]_{ex}$ or $[Ba^{2+}]_{ex}$ solution for Fig. 2 and 3 (minus Fig. 2e, 2f)**

**External**

| $CaCl_2$ | $BaCl_2$ | TEA-Cl | HEPES |
|---|---|---|---|
| 2 | 0 | 160 | 10 |
| 0 | 2 | 160 | 10 |

**pH 7.4 with TEA-OH**

**Internals**

| # | CsCl | $NMDG^+$ | EGTA | Mg-ATP | Li-GTP | HEPES |
|---|---|---|---|---|---|---|
| **1** | 110 | 0 | 10 | 3 | 0.6 | 10 |
| **2** | 0 | 110 | 10 | 3 | 0.6 | 10 |

**[1]pH 7.2 with CsOH**
**[2]pH 7.2 with HCl**

**$[Ca^{2+}]_{ex}$ +/- $[Na^+]_{ex}$ solutions for Fig. 2e, 2f**

**External**

| $CaCl_2$ | NaCl | $NMDG^+$ | TEA | HEPES |
|---|---|---|---|---|
| 2 | 0 | 135 | 25 | 10 |
| 2 | 135 | 0 | 25 | 10 |

**pH 7.4 with TEA-OH**

**Internals**

| # | CsCl | $NMDG^+$ | EGTA[#] | Mg-ATP | Li-GTP | HEPES |
|---|---|---|---|---|---|---|
| **1** | 110 | 0 | 10 | 3 | 0.6 | 10 |

**[1]pH 7.2 with CsOH**

**Bi-ionic solutions for reversal potential expts., Fig. 4, 5a, 5b**

**External**

| $CaCl_2$ | TEA-Cl | HEPES |
|---|---|---|
| 4 | 155 | 10 |

**pH 7.4 with TEA-OH**

**Internals**

| # | CsCl | NaCl | KCl | LiCl | EGTA[#] | TEA-Cl | HEPES |
|---|---|---|---|---|---|---|---|
| **1** | 100 | 0 | 0 | 0 | 10 | 10 | 10 |
| **2** | 0 | 100 | 0 | 0 | 10 | 10 | 10 |
| **3** | 0 | 0 | 100 | 0 | 10 | 10 | 10 |
| **4** | 0 | 0 | 0 | 100 | 10 | 10 | 10 |

**pH 7.2 with XOH where X= Cs, Na, K, or Li.**
**[#] pH 8.0 with XOH**

**TABLE 2**
External and internal recording solutions (part 2)

**$[Ca2+]_{ex}$ dose response with 60 mM $[Na^+]_{ex}$, Fig. 5c-5f**

**External**

| in mM | $Ca^{2+}$ free | $CaCl_2$ | NaCl | EGTA | HEPES | Glucose |
|---|---|---|---|---|---|---|
| 1 | $1x10^{-9}$ | 0.01 | 60 | 1.246 | 10 | 26.3 |
| 2 | $1x10^{-7}$ | 1.00 | 60 | 2.236 | 10 | 20.4 |
| 3 | $1x10^{-5}$ | 1.00 | 60 | 1.002 | 10 | 24.1 |
| 4 | $1x10^{-4}$ | 0.10 | 60 | 0 | 10 | 29.7 |
| 5 | $3x10^{-4}$ | 0.30 | 60 | 0 | 10 | 29.1 |
| 6 | $1x10^{-3}$ | 1.00 | 60 | 0 | 10 | 27.0 |
| 7 | $3x10^{-3}$ | 3.00 | 60 | 0 | 10 | 21.0 |
| 8 | $1x10^{-2}$ | 10.00 | 60 | 0 | 10 | 0.0 |

**pH 7.4 with TEA-OH**

**Internal**

| CsCl | EGTA | Mg-ATP | Li-GTP | HEPES |
|---|---|---|---|---|
| 110 | 10 | 3 | 0.6 | 10 |

**pH 7.4 with CsOH**

**Solutions for heart experiments Fig. 6d-6h, 7**

**External**

| # | $BaCl_2$ | NaCl | NMDG+ | TEA-Cl | $MgCl_2$ | HEPES |
|---|---|---|---|---|---|---|
| 1 | 2 | 100 | 0 | 50 | 1 | 10 |
| 2 | 2 | 0 | 100 | 50 | 1 | 10 |

[1]pH 7.9 with CsOH
[2]pH 7.9 with HCl

**Internals**

| # | CsCl | 4-AP | EGTA[#] | Mg-ATP | HEPES |
|---|---|---|---|---|---|
| 1 | 135 | 5 | 10 | 2 | 10 |

[1]pH 7.7 with CsOH

or 10 and 14 MΩ (heart cells). Only recordings with minimal leak (<10% of peak) and small current sizes (<500 pA) in HEK-293T cells were used due to loss of voltage clamp above 500 pA. Series resistance was compensated to 70% (prediction and correction, 10-$\mu$s time lag). Off-line leak subtraction was carried out using the Clampfit 10.1 software (Molecular Devices). Protocols for measuring the voltage sensitivity and kinetics and curve fitting data are described in Refs. 13, 14. The relative permeability of $P_{Ca}/P_x$, where $x$ is monovalent ion ($Li^+$, $Na^+$, $K^+$, and $Cs^+$), was calculated by the following bi-ionic Equation 1 (18),

$$\frac{P_{Ca}}{P_x} = \frac{[x]_i}{4[Ca]_o}\exp(E_{rev}F/RT)\{\exp(E_{rev}F/RT) + 1\} \quad \text{(Eq. 1)}$$

*Measurement of mRNA Expression of Exon 12a and Exon 12b Splice Variants Using qPCR*—qPCR[4] was carried out as described previously (14, 19, 20). RNA was extracted from

[4] The abbreviations used are: qPCR, quantitative PCR; aa, amino acid; MΩ, megohm; $NMDG^+$, *N*-methyl-D-glucamine; LVA, low voltage-activated; HVA, high voltage-activated.

**TABLE 3**
**Primers used for qPCR of control gene HPRT1, $LCa_v3$, $LNa_v1$ and $LNa_v2$**
$LCa_v3$ primer sets include universal sequence primers, exon 12a isoform-specific primers, and exon 12b isoform-specific primers. PCR efficiency (E), goodness of fit $R^2$ values, and slopes for the standard curves used to characterize qPCR primer pairs are shown in red.

| Real time RT primers: | | Amplification Length | length | Tm (°C) | GC% | qPCR E | R2 | Slope |
|---|---|---|---|---|---|---|---|---|
| Lymnaea HPRT1 5' | TGTAGAAGACATCATTGACACTGG | 145 | 24 | 53.86 | 42 | 90.4 | 0.985 | -3.576 |
| Lymnaea HPRT1 3' | GCCAATATAATCTGGTGCGTAAC | | 23 | 53.06 | 43 | | | |
| $LCa_v3$ Universal 5' | CAGAGTGACACAGATGTGCTACAG | 139 | 24 | 57.34 | 50 | 104.7 | 0.986 | -3.215 |
| $LCa_v3$ Universal 3' | GGTTATAGGATAAAGTGCCATGCT | | 24 | 54.14 | 42 | | | |
| $LCa_v3$ 12b 5' | CGCACCATGGACAATGTAGCAAC | 145 | 23 | 57.05 | 52 | 90.4 | 0.984 | -3.576 |
| $LCa_v3$ 12b 3' | CGTTAAGACGATCCTTGCAGGAG | | 23 | 57.82 | 52 | | | |
| $LCa_v3$ 12a 5' | CGCACCATGGACAATGTAGCAAC | 134 | 23 | 57.05 | 52 | 92.3 | 0.977 | -3.523 |
| $LCa_v3$ 12a 3' | CGATCACATTTACGGAATCCACCATC | | 26 | 57.29 | 46 | | | |
| $LNa_v1$ 5' | GCCTTGCTGCTCAGTTCTTT | 124 | 20 | 54.3 | 50 | 111.9 | 0.987 | -3.07 |
| $LNa_v1$ 3' | TCTTTACCTTGACCCAGTTACCA | | 23 | 52.85 | 43 | | | |
| $LNa_v2$ 5' | CCTCCATATTGCAATCCTAATTTC | 113 | 24 | 51.95 | 38 | 107.9 | 0.959 | -3.15 |
| $LNa_v2$ 3' | ATGTAGCTCACCATGTAAGGGATT | | 24 | 54.43 | 42 | | | |

entire juvenile and adult snails, where sexually immature juveniles have shell lengths of 1.0 to 1.5 cm, and reproduction-capable adults have shell lengths of 2.0 to 2.5 cm (21). qPCR primer sets (Table 3) were designed to selectively amplify universal and specific exon 12a and exon 12b splice variants of *Lymnaea* $Ca_v3$. The specificity of PCR primer pairs was initially assessed by comparing the size of PCR products amplified from a pooled cDNA library with those amplified from cloned cDNAs. PCR primer efficiency for each primer set was then determined by generating relative standard curves using the 1:5 serial dilutions of pooled cDNA (1:5, 1:25, 1:125, and 1:625) as template for real time RT-PCR amplification. For each dilution, triplicate reactions were carried out in rigid 96-well PCR plates (Bio-Rad), with each well containing 0.5 $\mu$l of serially diluted cDNA, 5 $\mu$l of SsoFast™ EvaGreen® Supermix (Bio-Rad), 0.5 $\mu$l of each 10 $\mu$M primer from a set, and 3 $\mu$l of water. PCR amplification, fluorescence reading, and melt curve analyses were done using a Bio-Rad C1000™ Thermal Cycler equipped with a CFX96TM Real-Time System and run by CFX Manager software (Bio-Rad). All cycle threshold values used for analysis were determined relative to the average cycle threshold value of the control gene, HPRT1 (hypoxanthine phosphoribosyltransferase 1).

## RESULTS

*Novel Spliced Turret Alters Monovalent Ion Permeability of Snail T-type Channels*—T-type channels diversified into three vertebrate genes but are rooted as a single T-type channel gene in extant relatives of animals spanning tissue and nervous system evolution (*Trichoplax* and cnidarians) and identified as the *$LCa_v3$* gene in the pond snail, *L. stagnalis* (13, 14). Expressible snail $LCa_v3$ channel resembles mammalian T-type channels in their rapid channel kinetics, and low threshold of activation for generating rhythmic pacemaker currents to threshold for eliciting action potential spikes (13). Snail channels also resemble particular mammalian T-type channels in their conserved and developmentally regulated exon splicing, such as with optional exons 8b and 25c, which confers membrane expression changes and changes to kinetic properties, respectively (14). We have identified unique exon splicing for exon 12 in the invertebrate T-type channel that spans from the S5 membrane helix of domain II, the extracellular loop, dubbed the "turret," to the

descending pore helix that projects into the pore toward the selectivity filter (Fig. 2*A*). Remarkably, the 3′-splice sites for exons 12a and 12b occur five amino acids upstream but do not include the invariant selectivity filter (Fig. 2*A*), whose residues define the channel's characteristic ion selectivity (22). Exon 12a is shorter (39 aa long) with a characteristic cysteine structure, $C_{xx}C \ldots C$, whereas exon 12b has a penta-cysteine structure $C \ldots C_xC \ldots C_xC$ and is longer (50 aa long) (Fig. 2*A*). Snail $LCa_v3$-12a and $LCa_v3$-12b were recorded with 2 mM $Ca^{2+}$ as the external charge carrier in transfected HEK-293T cells, using whole cell patch clamp as described previously (13, 14), with the cell culturing methods we describe in an on-line video publication (JoVE) (17). A notable difference for $LCa_v3$-12a compared with $LCa_v3$-12b in the ensemble of voltage-gated calcium currents was a large outward current with voltage steps above 0 mV (Fig. 2, *B* and *D*). We suspected that the large outward current with $LCa_v3$-12a was carried by the outflow of 110 mM $Cs^+$ from the intracellular patch pipette, a constituent normally present in the patch pipette to block $K^+$ currents. Replacement of 110 mM internal $Cs^+$ with equimolar impermeant monovalent cation *N*-methyl-D-glucamine ($NMDG^+$) eliminated most of the outward current for $LCa_v3$ isoforms, leaving a residual current, possibly carried by $NMDG^+$, but also the 0.6 mM $Li^+$ in the compound Li-GTP and other monovalent contaminants contained in the intracellular solution (Fig. 2, *C* and *D*). Calcium channels have a high affinity for $Ca^{2+}$ ions, and monovalent ions are normally excluded in the presence of physiological levels of extracellular calcium, $[Ca^{2+}]_{ex}$ (10). Thus, it was surprising to observe that $LCa_v3$-12a generated >15-fold greater peak inward currents in the presence of 2 mM $Ca^{2+}$ with physiological levels of $[Na^+]_{ex}$ at 135 mM, whereas $LCa_v3$-12b was significantly less permeable with only an ~2.5-fold increase (Fig. 2, *E* and *F*). With such a dramatic change in the pore's ion permeability for $LCa_v3$-12a, it is surprising that both snail $LCa_v3$-12a and -12b isoforms have completely overlapping biophysical properties, such as voltage sensitivities and kinetics of activation and inactivation (Fig. 3, *A* and *B*), as well as the size of the currents in divalent cations ($Ba^{2+}$ currents being ~1.3-fold larger than $Ca^{2+}$ currents) (Fig. 3*C*) and similar sensitivity to block by $Ni^{2+}$ ions (Fig. 3*D*). Outside of permeability changes, there is a notably faster recovery rate from inactivation (Fig. 3*E*) and slower deactivation rate for the $LCa_v3$-12a isoform (Fig. 3*F*). Yet, taking it all together (see Table 4), it is surprising how an extracellular turret, constituting ~1% of the channel's length, has remarkably little effect on the T-type channel while dramatically altering monovalent cation permeability.

*Snail T-type Channel with Exon 12a Is More Permeant to Sodium Ions than Calcium Ions*—To quantify ion permeability differences, we measured peak sizes of T-type channel currents generated in bi-ionic conditions with intracellular solutions containing 100 mM of differing monovalent ions ($Li^+$, $Na^+$, $K^+$, or $Cs^+$) in the presence of external calcium ions (4 mM $[Ca^{2+}]_{ex}$). We compared the more sodium-permeant snail $LCa_v3$-12a and snail $LCa_v3$-12b isoforms to the most sodium-impermeant human T-type channel, $Ca_v3.1$. Sizes of outward currents were elicited from a −110-mV holding potential in voltage steps from −90 to +80 mV in 5-mV increments (Fig. 4*A*). The relative permeability of monovalent ions followed the ion selectivity model by Eisenman *et al.* (23), where $Li^+ > Na^+ > K^+ > Cs^+$, and is consistent with the decreasing permeability with increasing crystal radii of monovalent ions from $Li^+ < Na^+ < K^+ < Cs^+$ ($A^o$) = 0.60, 0.95, 1.33, and 1.69, respectively (Fig. 4, *A* and *B*). The contribution of each monovalent ion to a change in reversal potential reflects its relative permeability to the reference external calcium ion. Calculating the relative $Li^+$, $Na^+$, $K^+$, and $Cs^+$ permeability in the bi-ionic Nernst equation reveals $P_{Ca}/P_x$ with approximate averages of 23, 32, 49, and 118 for $LCa_v3$-12a channels, 26, 41, 78, and 114 for $LCa_v3$-12b channels, and 45, 90, 140, and 155 for human $Ca_v3.1$ channels (Fig. 5*A*). $LCa_v3$ channels with the exon 12a turret are significantly more permeable to monovalent ions than $LCa_v3$ channels bearing the exon 12b turret. Both snail channel splice variants are much more sodium-permeant than human $Ca_v3.1$, which is considered the most sodium-impermeant of the three mammalian T-type channels, $Ca_v3.1$, $Ca_v3.2$, and $Ca_v3.3$ (10, 11). L-type channels are much more selective for calcium ions, and their monovalent ion permeability is barely detectable. L-type calcium channels are 10–60-fold more selective for calcium ions than T-type channels with relative $Li^+$, $Na^+$, $K^+$, and $Cs^+$ permeability ratios reported as $P_{Ca}/P_x$ of 424, 1170, 3000, and 4200 (9, 18). Another way to gauge the relative permeabilities is in the linear slope conductances between voltage steps from +70 to +80 mV, where the outward monovalent ion currents possess steeper conductance slopes in current voltage relations, reflecting the much greater observed outward monovalent current through snail $LCa_v3$-12a compared with snail $LCa_v3$-12b channels or human $Ca_v3.1$ (Fig. 5*B*). Monovalent ions such as sodium are competing with calcium ions for pore-binding sites (18), so we measured the changing peak amplitudes of the inward-permeating sodium current in 60 mM $Na^+_{ex}$ with 10-fold increment doses of extracellular calcium, in a range from $10^{-9}$ to $10^{-2}$ M. As calcium levels rose, there was an increased blocking of the $Na^+$ current by calcium ions (Fig. 5*C*), reflecting a decrement of the sodium current with increasing external calcium. A striking difference for channels with the exon 12a turret is a weak calcium blocking effect (44.5 ± 4.0%) compared with almost a complete block for channels with exon 12b turret (81.2 ± 1.6%) or human $Ca_v3.1$ channels (96.1 ± 1.6%) at 10 $\mu$M $[Ca^{2+}]_{ex}$ (Fig. 5*D*). Above 10 $\mu$M $[Ca^{2+}]_{ex}$, $Ca^{2+}$ out-competes sodium in the pore and the observed in current rises through $Ca_v3.1$ channels as calcium reaches physiological (millimolar) levels (Fig. 5*E*). Current sizes through $Ca_v3.1$ rise 9.1-fold from 10 $\mu$M to 10 mM external calcium, in the presence of a constant 60 mM $[Na^+]_{ex}$ reflecting the much greater permeability of the human $Ca_v3.1$ channel for calcium ions. The lack of calcium permeability of snail $LCa_v3$ channels is reflected in the 6.5- and 2.0-fold monotonic decline ($LCa_v3$-12a and $LCa_v3$-12b, respectively) in current size when calcium levels are rising between 10 $\mu$M and 10 mM external calcium (Fig. 5, *E* and *F*). The switch from a calcium block of $Na^+$ current to permeation and rise of calcium currents generates a characteristic U-shaped dose-response curve over the range of calcium concentrations for mammalian T-type channels (Fig. 5*C*) (10). The consequence of the extracellular turret from exon 12a is to alter T-type channel ion selectivity, shifting a preference to passage of sodium ions over calcium ions espe-

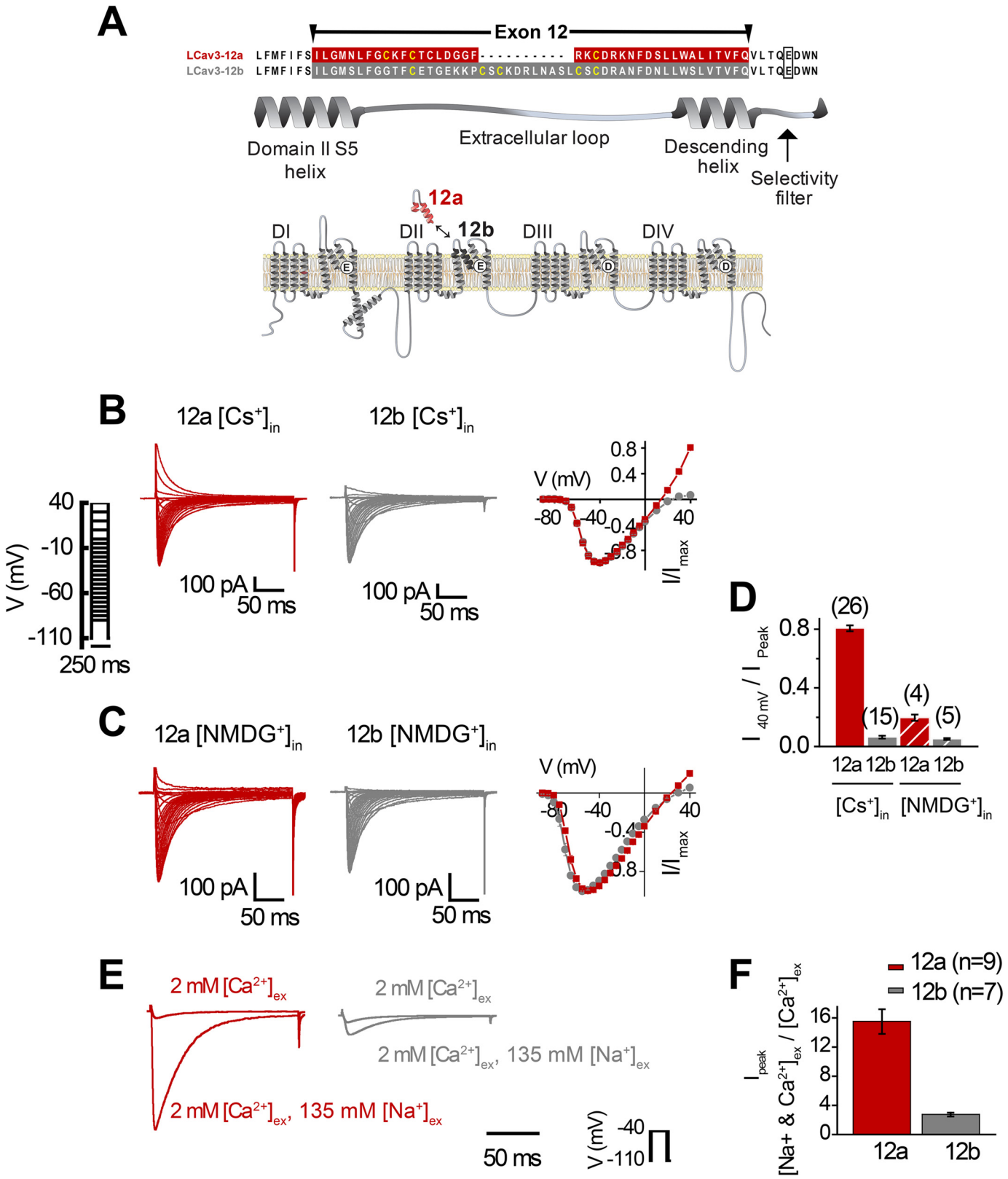


FIGURE 2. **Splicing of extracellular turret isoform (exon 12a) in the pore loop of domain II in snail LCa$_v$3 channels generates monovalent ion-permeant T-type channels.** *A,* aligned sequences illustrate mutually exclusive exons (12a and 12b) that correspond to a portion of the domain II S5 helix, the turret, and the descending helix that descends into the pore vestibule. *B,* dramatic difference in outward $Cs^+$ currents between LCa$_v$3-12a and -12b in 2 mM $[Ca^{2+}]_{ex}$ and 0.6 mM $[Li^+$-GTP] is mostly eliminated by replacement of 110 mM internal $Cs^+$ with equimolar impermeant $NMDG^+$ (*C*). Sample traces (*left*) and current voltage curves (*right*) are shown in *B* and *C*. *D,* ratio of maximum outward currents (at +40 mV) to peak inward current for *B* and *C*. *n* values are shown in *parentheses*. *E,* sample currents; *F, bar graph* illustrating the 15-fold peak inward current size with addition of 135 mM $[Na^+]_{ex}$ to 2 mM $[Ca^{2+}]_{ex}$ with LCa$_v$3-12a, compared with the ~2.5-fold change with LCa$_v$3-12b. Statistics for Fig. 2, *E* and *F*, are shown in Table 5.

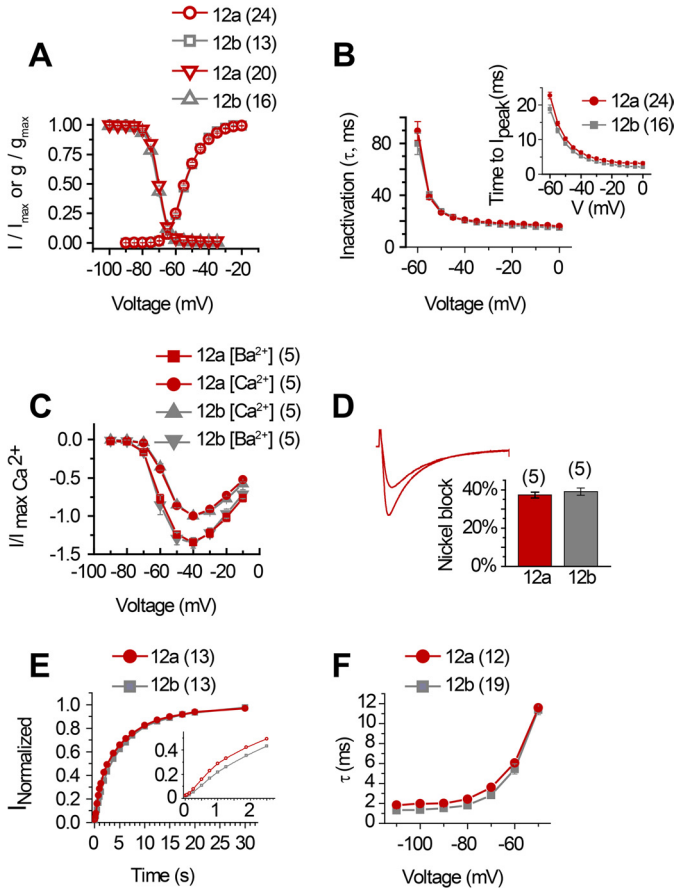


FIGURE 3. **Differing extracellular turrets in domain II P-loop (exons 12a and 12b) do not alter major features outside of monovalent ion permeability.** There were no major differences in most biophysical properties between $LCa_v3$-12a and $LCa_v3$-12b in 2 mM $[Ca^{2+}]_{ex}$, including the following: *A,* current-voltage relationship for activation and steady-state inactivation; *B,* inactivation kinetics and time to peak (*inset*); *C,* current size differences in 2 mM $[Ba^{2+}]_{ex}$ *versus* $[Ca^{2+}]_{ex}$, and *D,* blockade by 300 $\mu$M $Ni^{2+}$. A sample of the blocking effect for nickel for $LCa_v3$-12a is shown in the *inset* of *D*. A sample of a similar block of nickel for $LCa_v3$-12b is shown in Fig. 3, *A* and *B*, of Ref. 13. There are measurable differences in faster recovery rate from inactivation (*E*) and slower deactivation kinetics for $LCa_v3$-12a (*F*). *n* values are shown in *parentheses*. The differences in the rate of recovery is observed at the earliest time point, when the time scale range is limited from 0 to 2 s (*E, inset*). Statistics for Fig. 3 are shown in Table 4.

**TABLE 4**

**Comparison of the biophysical parameters for snail $LCa_v3$ channel currents recorded harboring either exon 12A or exon 12B in HEK-293T cells**

| | $LCa_v3$-12a | $LCa_v3$-12b | Significance | p value |
|---|---|---|---|---|
| **Activation** | | | | |
| $V_{0.5}$ (mV) | -53.63 ±0.35 (24) | -53.48 ±0.34 (13) | n.s. | 0.768 |
| Slope (mv) | 5.60 ±0.09 (29) | 5.46 ±0.14 (13) | n.s. | 0.348 |
| **Activation NMDG** | | | | |
| $V_{0.5}$ (mV) | -63.50 ±0.60 (4) | -67.40 ±0.78 (5) | ** | 0.004 |
| Slope (mv) | 6.00 ±0.01 (4) | 5.57 ±0.43 (5) | n.s. | 0.348 |
| **Inactivation** | | | | |
| $V_{0.5}$ (mV) | -70.21 ±0.38 (20) | -70.89 ±0.49 (16) | n.s. | 0.262 |
| Slope (mV) | 2.73 ±0.04 (20) | 2.93 ±0.08 (16) | * | 0.019 |
| **Activation kinetics** | | | | |
| TTP -55 mV (ms) | 14.68 ±0.63 (24) | 12.62 ±0.70 (16) | * | 0.035 |
| TTP -10 mV (ms) | 3.19 ±0.39 (24) | 2.35 ±0.12 (16) | n.s. | 0.088 |
| **Inactivation kinetics** | | | | |
| τ -55 mV (ms) | 38.40 ±1.67 (24) | 40.07 ±2.56 (16) | n.s. | 0.561 |
| τ -10 mV (ms) | 17.20 ±0.48 (24) | 15.67 ±0.56 (16) | * | 0.041 |
| **Deactivation kinetics** | | | | |
| τ -100 mV (ms) | 1.97 ±0.06 (12) | 1.37 ±0.05 (19) | *** | 0.000 |
| τ -60 mV (ms) | 6.05 ±0.30 (12) | 5.45 ±0.52 (19) | n.s. | 0.386 |
| **Inactivation Recovery** | | | | |
| % recovery (0.25 s) | 33.14 ±0.96 (13) | 26.19 ±0.86 (13) | *** | 0.000 |
| % recovery (4 s) | 93.69 ±0.69 (13) | 93.42 ±0.58 (13) | n.s. | 0.759 |
| $T_{0.5}$ (ms) | 921.49 ±22.45 (13) | 767.76 ±26.09 (13) | *** | 0.000 |

Values are expressed as mean +/- S.E.M. (numbers of cells used). TTP is the time to peak current. Statistical comparisons were done using a one-way ANOVA combined with a Student-Newman-Keuls post hoc test with * P<0.05, ** P<0.01 and *** P< 0.001; n.s., not significant.

cially at physiological concentrations and reducing the effectiveness of calcium ions to prevent sodium ions from permeating the channel pore. A summary of the monovalent and calcium permeability results are shown in Table 5.

*Sodium-permeant T-type Channel Is the Only Major Sodium Current in the Snail Heart*—We evaluated mRNA density of the differing extracellular turrets (exon 12a and 12b) in snail tissues by qPCR to determine where we could expect to find sodium-permeable T-type channels. The highest density of T-type channels was detected in the snail heart, where the expression pattern of $LCa_v3$ is exclusively the sodium-permeant $LCa_v3$-12a isoform and where the exon 12b isoform is not detectable (Fig. 6*A*). Whole animal $Ca_v3$ transcript levels steeply decline during embryonic development, and $LCa_v3$-12a continues to fall from juvenile to adults (Fig. 6*B*), which likely is largely attributable to the sharp decline of $LCa_v3$ expression specifically in the heart (Fig. 6*A*). The sodium-impermeant isoform $LCa_v3$-12b is of equal abundance as $LCa_v3$-12a in the brain but is almost exclusive in secretory reproductive tissue (prostate and albumen gland), where $LCa_v3$ expression rises from juvenile to adult animals (Fig. 6*A*). We examined the relative density of mRNA for all relevant voltage-gated cation channels comparing the heart and brain (Fig. 6*C*). Snail hearts only express two cation channel genes, the L-type channel $LCa_v1$ (24) and the highly sodium permeant T-type channel $LCa_v3$-12a (Fig. 6*C*). Brain-enriched genes such as the classical sodium channel serving to generate the action potential upstroke ($LNa_v1$ (15)) is completely lacking in the snail heart. Also, the snail heart does not express the brain-enriched synaptic non-L-type calcium channel $LCa_v2$ (25). Note the line break in the *y* axis scale in Fig. 6*C* to accommodate the scale of the $Na_v1$ sodium channel expression in the snail brain (~30-fold higher than control HPRT1 gene) that is dramatically above the range of expression of the other $LCa_v1$, $LCa_v2$, and $LCa_v3$ calcium channel genes (up to ~3-fold higher than control HPRT1 gene). The dramatic absence of expression of $LCa_v3$-12b and the highly brain-enriched $LNa_v1$ and $LCa_v2$ in the snail heart is evidence for the limited repertoire of four domain cation genes to $LCa_v3$-12a and $LCa_v1$ and a specialized signaling output in the snail heart that is highly different from the snail brain. We co-expressed and analyzed $LCa_v1$ (plus its required accessory $\beta$ and $\alpha_2\delta$ subunits) and $LCa_v3$-12a channels in HEK-293T cells, which is a configuration expected to emulate the major cation channels in snail cardiomyocytes. Voltage ramps generated from −100 to

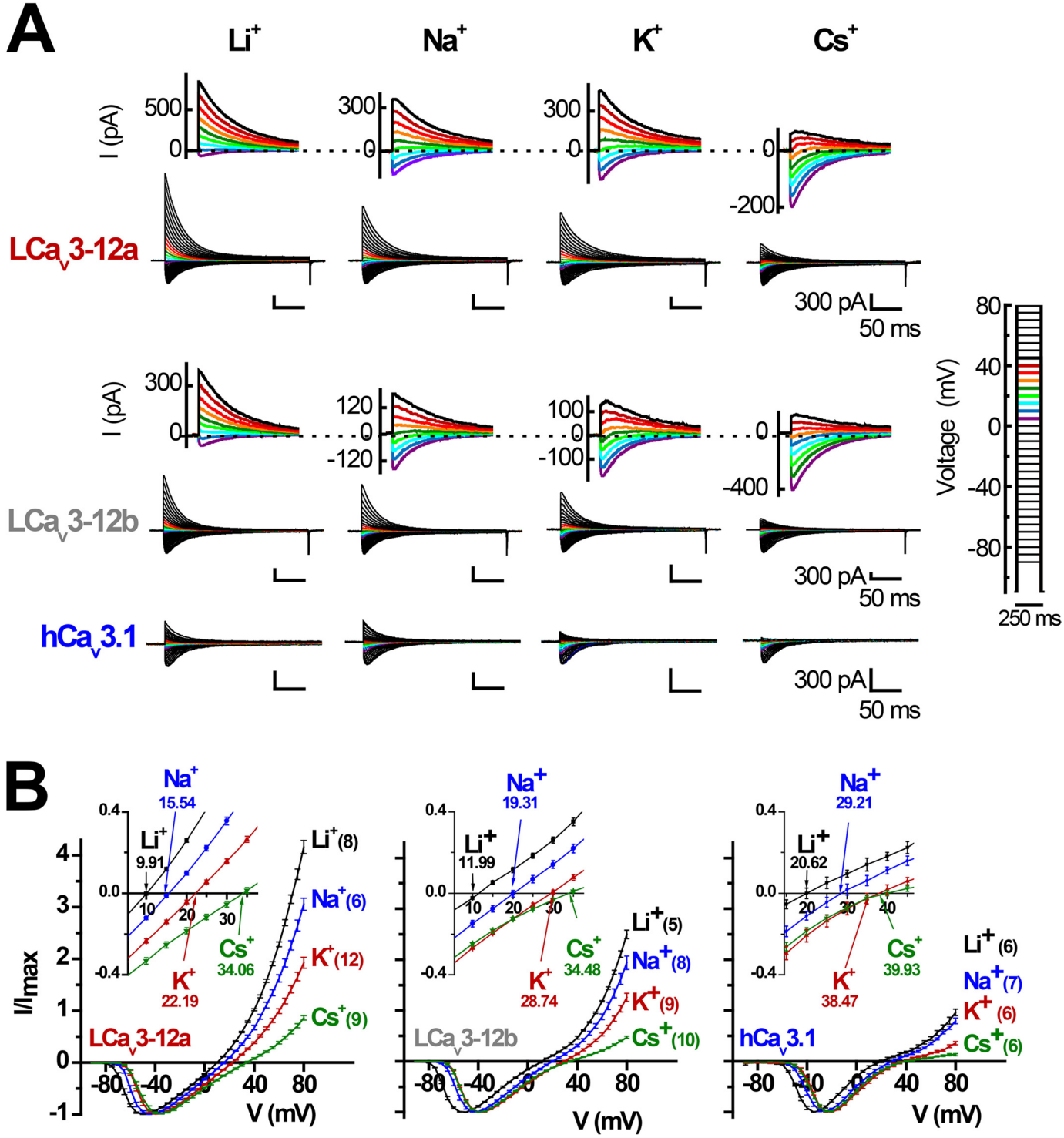


FIGURE 4. **Monovalent ion ($Li^+$, $Na^+$, $K^+$, and $Cs^+$) permeability through snail LCav3 T-type channels is especially dramatic with exon 12a compared with exon 12b extracellular turrets or human Cav3. 1 channels.** Inward calcium currents in 4 mM $[Ca^{2+}]_{ex}$ and outward monovalent T-type channel currents were generated with intracellular solutions containing 100 mM of $Li^+$, $Na^+$, $K^+$, or $Cs^+$ and elicited from a −110-mV holding potential in voltage steps from −90 to +80 mV in 5-mV increments. *A,* representative currents; *B,* their current-voltage relationships. *n* values are shown in *parentheses*. *A* or *B*, *inset*, close-up of currents crossing the reversal potential, with reversal potentials labeled in *B*. Statistics for Fig. 4 are shown in Table 5.

+80 mV separate low voltage-activated (LVA) T-type and high voltage-activated (HVA) L-type currents in 2 mM $[Ba^{2+}]_{ex}$ and impermeant $[NMDG^+]_{ex}$ at 100 mM (*black curve,* Fig. 6*D*). The high sodium permeation through $LCa_v3$-12a channels is revealed after replacing the 100 mM $NMDG^+$ with equimolar $Na^+$ (*red curve,* Fig. 6*D*). In the same recording, the HVA L-type current is unchanged when external $NMDG^+$ is replaced with $Na^+$, reflecting the channel's barium-selective currents and a lack of sodium permeability for L-type channels (Fig. 6*D*). A voltage ramp recording of adult snail cardiomyocytes (Fig. 6*F*) generates a remarkably similar profile of the sodium-permeant LVA T-type current and sodium-impermeant

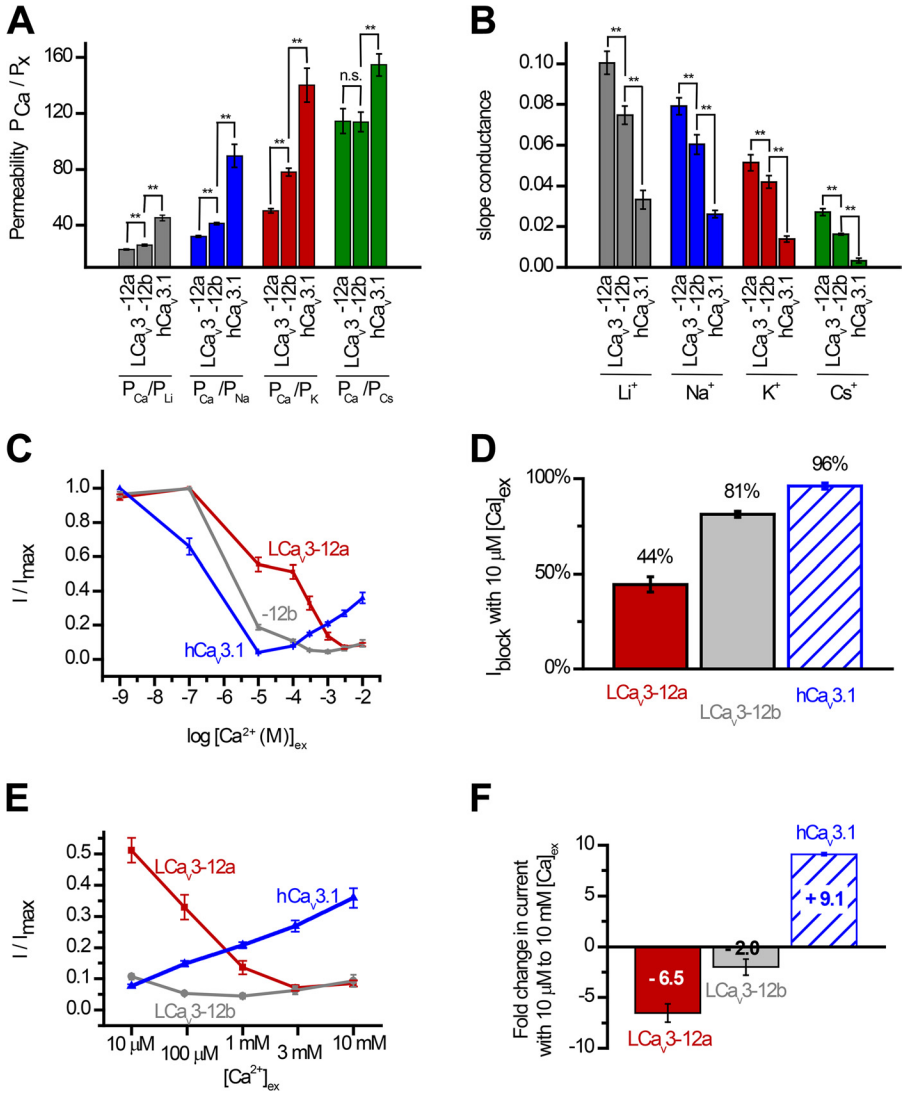


FIGURE 5. **Snail $LCa_v3$ channels with exon 12a are highly permeable to sodium ion and weakly permeant to calcium ions, compared with $LCa_v3$ channels with exon 12b or human Cav3. 1 channels.** *A,* relative permeabilities of calcium to monovalent cations ($P_{Ca}/P_x$) generated using reversal potentials (shown in Fig. 3*B*) inputted into a bi-ionic Nernst equation (see under "Experimental Procedures"). *B,* slope conductance of outward currents (shown in Fig. 3*B*) measured as the linear fit of currents generated from steps between +70 and +80 mV. *C,* increasing block of maximal ionic current ($I/I_{max}$) in 60 mM $Na^+$ external with increasing $[Ca^{2+}]_{ex}$ from $10^{-9}$ to $10^{-5}$ M reflects the competition between sodium and calcium ions to permeate the pore. *D, bar graph* illustrates the weak block of $LCa_v3$-12a channel current (44%) compared with $LCa_v3$-12b (81%) and human $Ca_v3.1$ (96%) channels at 10 $\mu$M $[Ca^{2+}]_{ex}$. *E,* X-scale shown for calcium dose-response curves (*C*) limited to rise in $[Ca^{2+}]_{ex}$ from 10 $\mu$M to 10 mM with corresponding *bar graph* (*F*), reflecting the dramatic fold decrease (×6.5 and ×2.0) in calcium permeability with snail $LCa_v3$-12a and -12b channels, respectively, compared with the dramatic fold increase (×9.1) in calcium current through the physiological range for external calcium ions. Statistical comparisons in *A* and *B* were done using a one-way analysis of variance combined with a Student-Newman-Keuls post hoc test with the following: *, $p < 0.05$; **, $p < 0.01$, and ***, $p < 0.001$; *n.s.*, not significant. Statistics for Fig. 5 are shown in Table 5.

HVA L-type current. The ~11-fold increase in size of the combined sodium and barium LVA current, upon addition of $Na^+$ ions, is identical in cells transfected with $LCa_v3$-12a channels and the endogenous LVA T-type current in cardiomyocytes (Fig. 6*H*). On the contrary, the ~2-fold current increase in HEK cells transfected with $LCa_v3$-12b (Fig. 6, *E* and *H*) or human $Ca_v3.1$ (Fig. 6, *G* and *H*) is not reflected in the T-type currents of cardiomyocytes, corroborating the qPCR data that $LCa_v3$-12a is the exclusive T-type isoform in the snail heart. The similarity between cardiomyocytes and transfected $LCa_v3$-12a/$LCa_v1$ channels is also revealed in the makeup of current ensembles initiated from differing holding potentials (Fig. 7*A*). We used 2 mM $Ba^{2+}$ and 100 mM $Na^+$ external solution to separate the kinetics of the slow barium L-type currents from the fast T-type currents mostly carried by sodium ions. A holding potential of −60 mV will inactivate T-type sodium currents, leaving a residual L-type current (*gray color*) and a mostly pure T-type sodium current (*red color*) from the difference current generated from −110 and −60 mV holding potentials (Fig. 7*A*). We examined drug responses of currents in cardiomyocytes elicited by voltage ramp (Fig. 7, *B* and *C*). Pharmacologically, we could separate the L-type from the T-type current using 1 $\mu$M isradipine, but both the L-type and T-type currents were similarly blocked by nickel and mibefradil (Fig. 7, *B* and *C*). The sum of the electrophysiological data for cardiomyocytes (current kinetics, drug block, and sodium permeability) (Figs. 6 and 7) is consistent with the mRNA expression profiles in the heart,

**TABLE 5**

**Monovalent ion and calcium permeability parameters for snail $LCa_v3$–12a or $LCa_v3$–12ba channel or human $Ca_v3.1$ channel currents expressed in HEK-293T cells**

| reversal potentials : | Li | s.e.m. | n | Na | s.e.m. | n | K | s.e.m. | n | Cs | s.e.m. | n |
|---|---|---|---|---|---|---|---|---|---|---|---|---|
| Erev $LCa_v3$-12a | 9.91 | 0.27 | 8 | 15.54 | 0.31 | 6 | 22.19 | 0.44 | 12 | 34.06 | 1.02 | 9 |
| Erev $LCa_v3$-12b | 11.99 | 0.33 | 5 | 19.31 | 0.27 | 5 | 28.74 | 0.65 | 9 | 34.48 | 1.10 | 10 |
| Erev $Ca_v3.1$ | 20.62 | 0.72 | 6 | 29.21 | 1.84 | 7 | 38.47 | 1.82 | 6 | 39.93 | 1.58 | 6 |

| permeabilities : | $P_{Ca}/P_{Li}$ | s.e.m. | n | $P_{Ca}/P_{Na}$ | s.e.m. | n | $P_{Ca}/P_{K}$ | s.e.m. | n | $P_{Ca}/P_{Cs}$ | s.e.m. | n |
|---|---|---|---|---|---|---|---|---|---|---|---|---|
| $P_{Ca}/P_x$ $LCa_v3$-12a | 22.74 | 0.41 | 8 | 32.01 | 0.71 | 6 | 50.25 | 1.56 | 12 | 114.51 | 8.85 | 9 |
| $P_{Ca}/P_x$ $LCa_v3$-12b | 25.89 | 0.59 | 5 | 41.32 | 0.75 | 6 | 78.04 | 2.81 | 9 | 113.84 | 6.97 | 10 |
| $P_{Ca}/P_x$ $Ca_v3.1$ | 45.28 | 2.11 | 6 | 89.56 | 8.21 | 6 | 140.16 | 12.02 | 5 | 154.65 | 7.99 | 5 |

| slope conductance : | Li | s.e.m. | n | Na | s.e.m. | n | K | s.e.m. | n | Cs | s.e.m. | n |
|---|---|---|---|---|---|---|---|---|---|---|---|---|
| outward $g_X$ $LCa_v3$-12a | 0.100 | 0.0057 | 8 | 0.079 | 0.0042 | 5 | 0.051 | 0.0037 | 12 | 0.027 | 0.0017 | 8 |
| outward $g_X$ $LCa_v3$-12b | 0.075 | 0.0046 | 3 | 0.060 | 0.0047 | 8 | 0.042 | 0.0032 | 5 | 0.014 | 0.0008 | 11 |
| outward $g_X$ $Ca_v3.1$ | 0.026 | 0.0018 | 8 | 0.033 | 0.0046 | 7 | 0.014 | 0.0014 | 8 | 0.0033 | 0.0012 | 8 |

| $[Ca]_{ex}$ doses with 60 mM $[Na^+]_{ex}$ | $LCa_v3$-12a % current | | | $LCa_v3$-12b % current | | | $hCa_v3.1$ % current | | |
|---|---|---|---|---|---|---|---|---|---|
| log $[Ca]_{ex}$ | block | s.e.m. | n | block | s.e.m. | n | block | s.e.m. | n |
| -9 | 5.19% | 1.61% | 7 | 3.47% | 1.60% | 6 | 0.00% | 0.00% | 4 |
| -7 | 0.00% | 0.00% | 7 | 0.21% | 0.16% | 6 | 34.10% | 4.78% | 4 |
| -5 | 44.46% | 4.03% | 7 | 81.22% | 1.58% | 6 | 96.06% | 0.49% | 4 |
| -4 | 48.80% | 4.02% | 7 | 89.31% | 0.95% | 6 | 92.27% | 0.50% | 4 |
| -3.52 | 67.08% | 3.99% | 7 | 94.72% | 0.52% | 6 | 85.15% | 0.88% | 4 |
| -3 | 86.40% | 2.18% | 7 | 95.55% | 0.83% | 6 | 79.24% | 1.02% | 4 |
| -2.52 | 92.94% | 0.95% | 7 | 93.68% | 1.32% | 6 | 73.11% | 1.80% | 4 |
| -2 | 91.49% | 1.03% | 7 | 90.65% | 1.99% | 6 | 64.10% | 3.17% | 4 |

| | Current increase (fold) | s.e.m. | n |
|---|---|---|---|
| $LCa_v3$-12a | 15.40 | 0.83 | 5 |
| $LCa_v3$-12b | 2.53 | 0.10 | 7 |
| $hCa_v3.1$ | 1.27 | 0.09 | 4 |

which indicate an exclusive expression of sodium-permeant $LCa_v3$-12a and sodium-impermeant $LCa_v1$ channels.

*Alternatively Spliced Turrets for Generating Sodium-permeable T-type Channels Are Widespread in Protostome Invertebrates*—Analyses of $Ca_v3$ genomic sequences reveal that alternative splicing of exon 12 that we discovered in the snail *L. stagnalis* is widely present but limited to protostomes (*i.e.* non-echinoderm invertebrates) (Figs. 8 and 9 and Table 6). Exon 12a is characteristically short (38–46 aa long, average = 40.7 aa) with a nearly invariant tri-cysteine structure, *CXXC . . . C* (Fig. 8). Exon 12b has a penta-cysteine structure C . . . CXC . . . CXC (most protostomes) or CXXC . . . C . . . CXC (some nematodes) and is always longer (range, 48–55 aa long; average = 52.1 aa) than exon 12a (Fig. 9). The three vertebrate T-type channels, $Ca_v3.1$, $Ca_v3.2$, and $Ca_v3.3$, have an exon 12 with only one conserved cysteine (Fig. 8) compared with three and five cysteines in invertebrate exons 12a (Fig. 8) and 12b (Fig. 9), respectively. Paradoxically, the vertebrate exon 12 resembles the shorter exon 12a of invertebrates in size (38–39 aa long, average = 38.7 aa) which in snail $LCa_v3$ we have shown imparts the properties of extreme sodium ion permeability for exon 12a-containing T-type channels.

## DISCUSSION

*Unique Splicing of Exon 12 in Invertebrate T-type Channels*—We have functionally characterized the first nonvertebrate T-type calcium channel (13), which reveals a high conservation of quintessential features of vertebrate $Ca_v3.1$ and $Ca_v3.2$ T-type channels, including a similar low voltage range of activity with a peak current at −40 to −35 mV, with similar rapid activation and inactivation kinetics and slow deactivation kinetics. Also conserved is developmentally regulated splicing where T-type channels that lack exon 25c are highly down-regulated from embryo to adult animals, leading to a battery of biophysical changes among $LCa_v3$, $Ca_v3.1$, and $Ca_v3.2$ (14). We also found that the presence of optional exon 8b in the I-II linker specifically down-regulates the level of protein expression of snail T-type channels in a manner consistent with $Ca_v3.1$ (14). Here, we describe unique exon splicing that generates highly sodium-permeant T-type channels utilizing an alternative exon 12a, which spans the extracellular turret of domain II upstream of the highly conserved EEDD selectivity filter of T-type channels.

We show that invertebrate $LCa_v3$ T-type channels will generate large outward currents in the presence of 100 mM intracellular monovalent ions accompanying the large driving force at high voltage steps much more so than human $Ca_v3.1$, while also generating an inward calcium current in the presence of 4 mM extracellular calcium ions at voltage steps below the reversal potential (Figs. 2 and 4). Permeability of monovalent ions decreases with increasing ion diameter size where $Li^+ > Na^+ = K^+ > Cs^+ > NMDG^+$. All T-type channels pass sodium ions when external calcium concentration is at exquisitely low levels (<10 $\mu$M external calcium ions). However, the sodium current through human $Ca_v3.1$ has less physiological relevance because it is almost completely blocked (96%) by low (10 $\mu$M) external calcium. With rising external calcium concentrations to physiological levels, nearly all of the current through human $Ca_v3.1$ is carried by calcium (Fig. 5). The snail T-type channel isoforms, especially those harboring exon 12a, are not calcium-selective like human $Ca_v3.1$. Calcium ions are not effective at blocking the sodium current at 10 $\mu$M external calcium, with snail T-type channels with exon 12a resisting the calcium block (44%), much more than isoforms with exon 12b (81%) or human $Ca_v3.1$ (96%) (Fig. 5). Increasing external $Ca^{2+}$ above 10 $\mu$M to physiological (millimolar) levels does not generate the larger calcium currents for $LCa_v3$ as is reflected in the "U" shape calcium dose-response curve of human $Ca_v3.1$ (10). Rather, the total current size dramatically falls monotonically (6.5-fold) for snail channels harboring exon 12a reflecting their reduced affinity for $Ca^{2+}$ in the pore that allows for greater permeability of $Na^+$ ions (Fig. 5).

The extreme sodium permeability of $LCa_v3$-12a is evident in voltage ramp-generated currents with amplitudes that are ~11-fold greater when external $Na^+$ replaces impermeant cation $NMDG^+$ in the presence of barium. The sodium permeability is not evident in the co-expressed snail L-type ($LCa_v1$) channel in the same voltage ramp and a much reduced (~2-fold instead of ~11-fold) sodium permeability for $LCa_v3$ channels harboring exon 12b (Fig. 6). Snail heart cells only express T-type channels with exon 12a and express the same sodium-permeable T-type current as the *in vitro* expressed gene, resembling its fast kinetics, low voltage of activation, nickel (millimolar) and mibefradil (millimolar) sensitivity, and isradipine (micromolar) insensitivity (Figs. 6 and 7).

*Unique Functions for Highly Sodium-permeant (Exon 12a) and Less Sodium-permeant (Exon 12b) T-type Channels*—The distinct tissue expression patterns of $LCa_v3$ exons 12a (heart and muscle) and 12b (secretory glands) suggest specialized

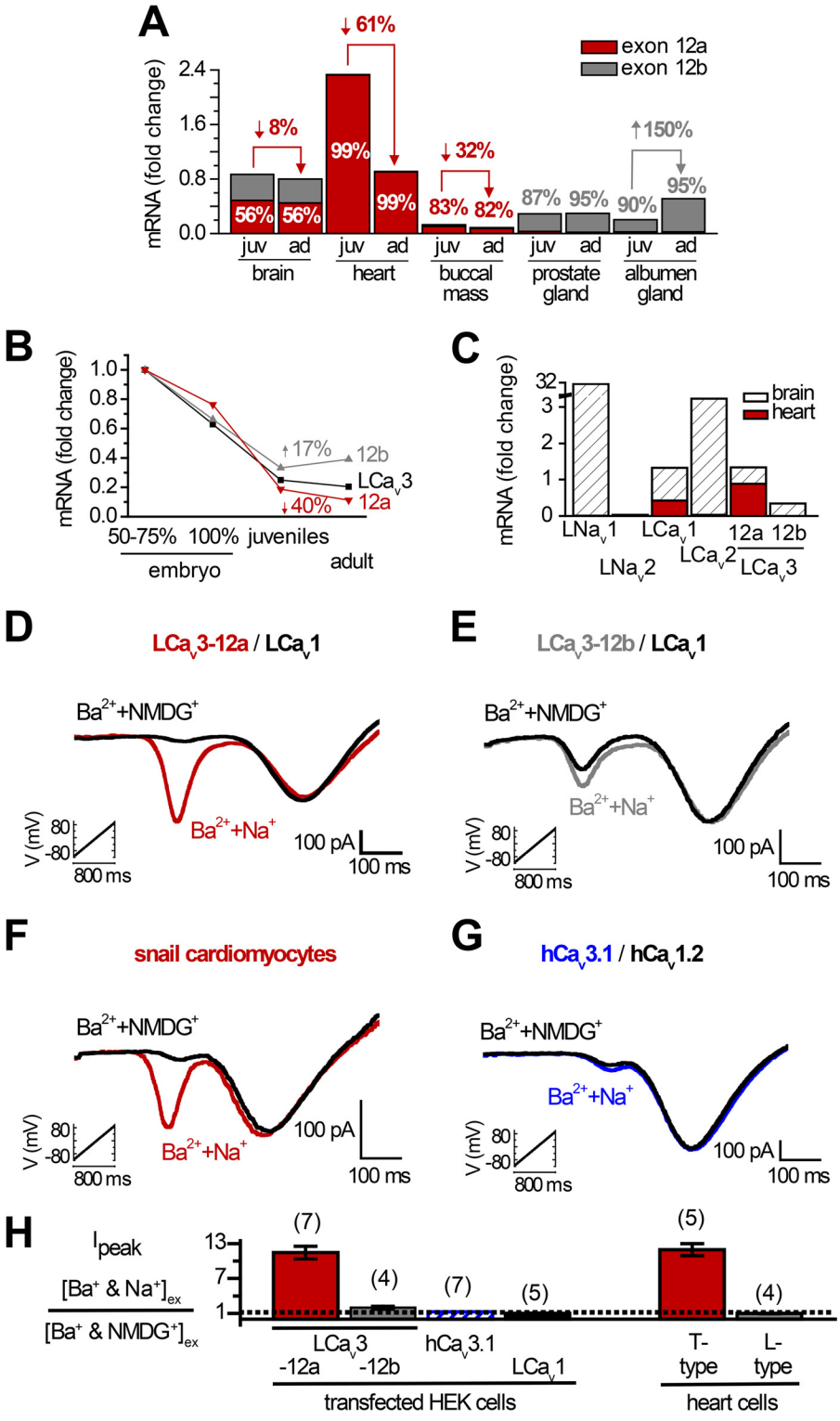


FIGURE 6. **Snails express two cardiac cation currents, the highly sodium-permeant T-type channel $LCa_V3$ and the calcium-selective L-type channel $LCa_V1$.** *A–C*, quantitative RT-PCR standardized to *Lymnaea* HPRT1 control gene. *A*, relative mRNA expression levels of exon 12a and 12b in juvenile (*juv*) and adult (*ad*) snails, reflecting the almost exclusive expression of exon 12a in the snail heart and exon 12b in prostate and albumen glands. *B*, dramatic decline in $LCa_V3$ channel expression in whole animals can mostly be attributed to the decline of $LCa_V3$-12a expression in the developing heart. *C*, snail hearts lack mRNA expression of any sodium channel gene ($LNa_V1$ and $LNa_V2$). Snail hearts also lack any expression of the $LCa_V2$ synaptic non-L-type channel or the $Ca_V3$ T-type channel gene with exon 12b. Note the break in the *y* axis scale, illustrating that the range of expression of the sodium channel gene of $LNa_V1$ in the snail brain is ~30-fold higher than the control HPRT1 gene, compared with the low levels of expression of the other calcium channel genes (which vary up to ~3-fold higher than the control HPRT1 gene). *D–G*, ramp protocols (−110 to +100 mV in 1 s) carried out in the presence of external solutions as follows: 2 mM $Ba^{2+}$ and 100 mM $Na^+$ ions or 2 mM $Ba^{2+}$ and 100 mM $NMDG^+$ reveal a covert sodium-permeant, T-type current superimposed on the $Ba^{2+}$ current in cardiomyocytes in the presence of a sodium-impermeant, L-type current (*F*). The sodium-permeant T-type currents in cardiomyocytes are indistinguishable from mammalian HEK-293T cells transfected with $LCa_V3$ with exon 12a with co-expression of $LCa_V1$ and accessory subunits ($\alpha_2\delta$ and $\beta_{2a}$) (*D*). *E*, $LCa_V3$ with exon 12b; *G*, human $Ca_V3.1$ has some $Na^+$ permeability but is not as $Na^+$-permeant as the $LCa_V3$-12a variant expressed in cardiomyocytes. *H*, *bar graph* ± S.E., including sample data in *D–G*.

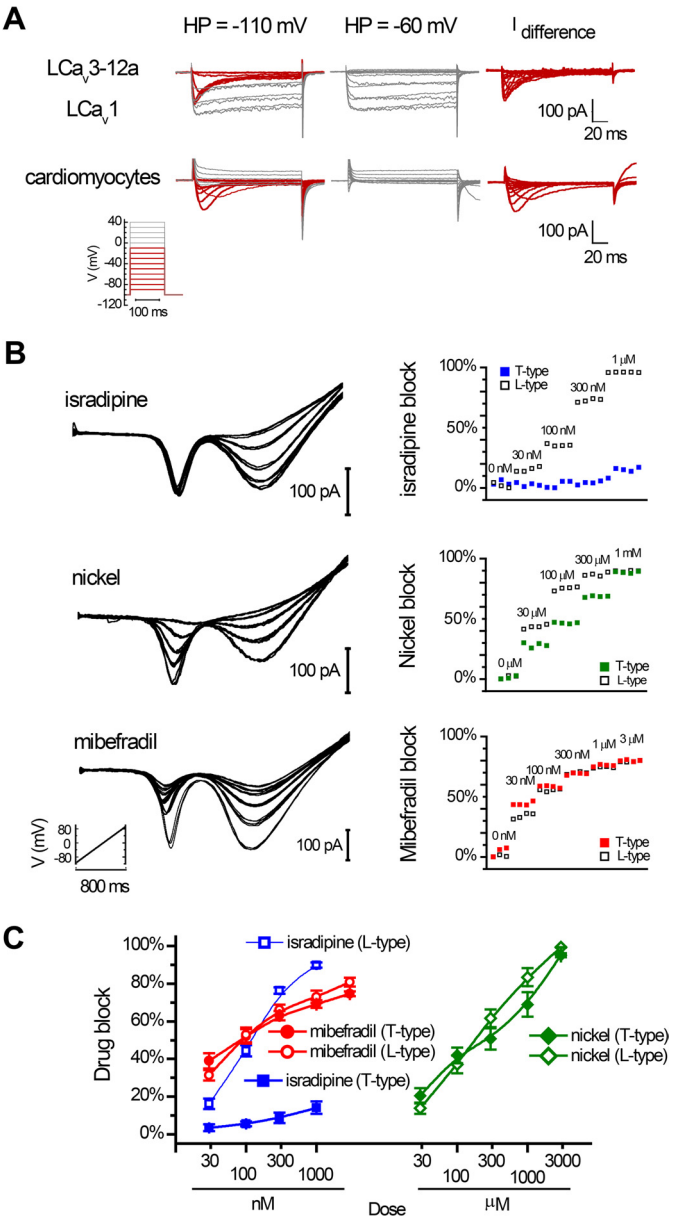


FIGURE 7. **Separation of snail cardiac LCa$_v$3-12a (T-type) and LCav1 (L-type) currents using holding potentials and drugs (isradipine, mibefradil, and nickel) in whole cell patch clamp recording.** *A,* fast T-type currents (*red color*) isolated by difference current in 2 mM $[Ba^{2+}]_{ex}$ and 100 mM $[Na^{+}]_{ex}$ with a holding potential (*HP*) of −110 mV *versus* −60 mV in whole cell recording of native LCav3/LCav1 channel currents in snail cardiomyocytes. *B,* ramp protocols (−110 to +100 mV in 800 ms) carried out in the presence of external solutions 2 mM $[Ba^{2+}]_{ex}$ and 100 mM $[Na^{+}]_{ex}$ and differing doses of drug perfused on cardiomyocytes. Isradipine at 1 μM is a specific blocker of L-type currents, whereas mibefradil and nickel are nonspecific blockers of L-type and T-type currents. *C,* dose-response curves ± S.E. for isradipine ($n$ = 6), mibefradil ($n$ = 8), and nickel ($n$ = 8); sample data are shown in *B*.

roles of different permeable T-type channels in different cell types. T-type channel transcript levels steeply decline during embryonic development through adulthood, reflected by a sharp decline in LCa$_v$3-12a expression in juvenile to adult heart (Fig. 6). A down-regulation of LCa$_v$3-12a may relate to allometric scaling during development, where more prominent LCa$_v$3 currents are found in smaller animals (non-adults) coinciding with faster heart rhythms (26). Expression of LCa$_v$3-12a isoform indicates a significantly slower deactivation rate and faster recovery rate from inactivation when compared with LCa$_v$3-12b (Fig. 3). This is consistent with LCa$_v$3-12a and adaptations in the snail heart, where a slower deactivation would serve to prolong the repolarization phase of the cardiac action potential, and a faster inactivation recovery prevents rundown between heart beats due to cumulative inactivation. Snails have only one (nonspecialized) sodium channel gene (Na$_v$1), compared with 10 in vertebrates, and this gene is only expressed in the snail brain and is not expressed in the snail heart (Fig. 6) (15). Thus, LCa$_v$3-12a is the only voltage-gated sodium channel generating pacemaker currents in ventricular cells of the primitive two-chambered snail heart, which lacks the appearance of specialized vertebrate sodium channels, like Na$_v$1.5 and other neuronal Na$_v$ channels for fast conduction of heart rhythms.

The more calcium-selective isoform LCa$_v$3-12b is of equal abundance to LCa$_v$3-12a in the brain, and it is the almost exclusive transcript associated with reproductive tissue of the hermaphroditic snail (prostate = male organ and albumen gland = female organ) (Fig. 6). The rise in transcripts of LCa$_v$3-12b from juvenile to adults (Fig. 6) coincides with sexual maturation where the albumen gland takes up a role secreting factors that facilitate egg mass formation (27). Our observations of a much faster deactivation rate and a slower recovery rate from inactivation of LCa$_v$3-12b channels promotes the typical pulsatile, burst firing of vertebrate T-type channels, where the rise in intracellular calcium may contribute to pacemaking and possibly also to excitation-secretion coupling (14).

Snail LCa$_v$3 (like its vertebrate counterparts) also has prominent "window" currents, where an estimated 1–2% of available channels are open at rest (13). LCa$_v$3-12a variants are highly abundant in the brain and likely contribute to reported persistent sodium currents (28, 29) serving as a significant sodium leak conductance (30). Even though highly sodium-permeant T-type channels are likely widespread in invertebrates, it would be hard to discern them with voltage-gated sodium channel currents if you were not looking for them. Drugs are not selective in most invertebrates, like snails that are insensitive to classical sodium blockers such as tetradotoxin (15), and neither are snail T-type channels easily discernible by $Ni^2$ block (13). Some species, including nematodes like *Caenorhabditis elegans*, lack a sodium channel (Na$_v$) gene in their genomes (31), which means that their sodium-permeant T-type channels with exon 12a likely serve as a critical source for generating sodium-dependent spikes in these organisms. Most invertebrates do contain gene homologs of hyperpolarization-activated cyclic nucleotide-gated channels, which presumably contribute to sodium currents in invertebrate pacemaker rhythms (32). A hyperpolarization-activated cyclic nucleotide-gated channel homolog is also notably absent in *C. elegans* (31, 32), which limits the possibilities of sodium current generating spikes in these animals from the conventional palette of ion channel genes. We suggest that T-type sodium channels have a role to play in lieu of sodium channels in *C. elegans*.

*Evolutionary Adaptations of the Domain II Turret*—A pattern of evolution of the extracellular turret in domain II of T-type channel is evident in their phylogeny (Fig. 10). The Ca$_v$3 T-type channel class first appeared in the most primitive multicellular animals, as low voltage-activated calcium-selective

**TABLE 6**

**Features of exons 11 and 12 of Cav3 channel homologs in sequenced metazoan genomes**

| Phylum | Subphylum/Class/Order | Species | Common Name | 11/12a Intron | Exon Size 12a | Exon Size 12a | # Cysteines 12a | # Cysteines 12b |
|---|---|---|---|---|---|---|---|---|
| Chordata | Subphylum Vertebrata | *Homo sapiens* | human | ✓ | 38 | | 1 | |
| Chordata | Subphylum Vertebrata | *Xenopus tropicalis* | Western Clawed Frog | ✓ | 38 | | 1 | |
| Chordata | Subphylum Vertebrata | *Takifugu rubripes* | Japanese pufferfish | ✓ | 38 | | 1 | |
| Chordata | Subphylum Vertebrata | *Homo sapiens* | human | ✓ | 39 | | 1 | |
| Chordata | Subphylum Vertebrata | *Xenopus tropicalis* | Western Clawed Frog | ✓ | 39 | | 1 | |
| Chordata | Subphylum Vertebrata | *Takifugu rubripes* | Japanese pufferfish | ✓ | 39 | | 1 | |
| Chordata | Subphylum Vertebrata | *Takifugu rubripes* | Japanese pufferfish | ✓ | 39 | | 1 | |
| Chordata | Subphylum Vertebrata | *Homo sapiens* | human | ✓ | 39 | | 1 | |
| Chordata | Subphylum Vertebrata | *Xenopus tropicalis* | Western Clawed Frog | ✓ | 39 | | 1 | |
| Chordata | Subphylum Vertebrata | *Takifugu rubripes* | Japanese pufferfish | ✓ | 39 | | 1 | |
| Chordata | Subphylum Vertebrata | *Takifugu rubripes* | Japanese pufferfish | ✓ | 39 | | 1 | |
| **Vertebrates (exon 12a = 38-39 aa with uni-cysteine motif)** | | | | **AVG** | **38.7** | | **1.0** | |
| sodium-impermeant calcium channels | | | | **SE** | **0.1** | | | |
| | | | | **RANGE** | **38-39** | | | |
| Chordata | Subphylum Cephalochordata | *Branchiostoma floridae* | Lancelet or Amphioxus | ✓ | 41 | | 2 | |
| Chordata | Subphylum Urochordata | *Ciona intestinalis* | Sea (Vase) Squirt | ✓ | 39 | | 3 | |
| Chordata | Subphylum Urochordata | *Oikopleura dioica* | marine tunicate | | 39 | | 3 | |
| Hemichordata | Class Enteropneusta | *Saccoglossus kowalevskii* | acorn worm | ✓ | 39 | | 3 | |
| Echinodermata | Class Echinoidea | *Strongylocentrotus purpuratus* | California Purple Sea Urchin | ✓ | 38 | | 3 | |
| Annelida | Class Clitellata | *Helobdella robusta* | glossiphoniid leech | ✓ | 41 | | 3 | |
| Annelida | Class Clitellata | *Lumbricus rubellus* | redworm earthworm | ✓ | 40 | | 3 | |
| Annelida | Class Polychaeta | *Capitella teleta* | polychaete worm | ✓ | | 50 | | 5 |
| Mollusca | Class Gastropoda / Heterobranchia | *Lymnaea stagnalis* | giant pond, freshwater snail | ✓ | 39 | 50 | 3 | 5 |
| Mollusca | Class Gastropoda / Heterobranchia | *Biomphalaria glabrata* | Bloodfluke Planorb, freshwater snail | ✓ | 39 | 50 | 3 | 5 |
| Mollusca | Class Gastropoda / Heterobranchia | *Aplysia californica* | California Sea Hare | ✓ | 46 | 51 | 3 | 5 |
| Mollusca | Class Gastropoda / Patellogastropoda | *Lottia gigantea* | Owl Limpet | ✓ | 38 | 51 | 3 | 5 |
| Arthropoda | Class Insecta / Coleoptera | *Tribolium castaneum* | red flour beetle | ✓ | 38 | 55 | 3 | 5 |
| Arthropoda | Class Insecta / Diptera | *Drosophila melanogaster* | fruit fly | ✓ | 38 | 55 | 3 | 5 |
| Arthropoda | Class Insecta / Diptera | *Drosophila mojavensis* | fruit fly | ✓ | 38 | 55 | 3 | 5 |
| Arthropoda | Class Insecta / Diptera | *Anopheles gambiae* | African malarial mosquito | ✓ | 40 | 55 | 3 | 5 |
| Arthropoda | Class Insecta / Diptera | *Aedes aegypti* | yellow fever mosquito | ✓ | 42 | 55 | 3 | 5 |
| Arthropoda | Class Insecta / Diptera | *Culex quinquefasciatus* | southern house mosquito | ✓ | 41 | 55 | 3 | 5 |
| Arthropoda | Class Insecta / Lepidoptera | *Danaus plexippus* | monarch butterfly | ✓ | 39 | 55 | 3 | 5 |
| Arthropoda | Class Insecta / Hymenoptera | *Apis mellifera* | Western honey bee | ✓ | 40 | 52 | 3 | 5 |
| Arthropoda | Class Insecta / Hymenoptera | *Nasonia vitripennis* | jewel wasp | ✓ | 40 | 52 | 3 | 5 |
| Arthropoda | Class Insecta / Hemiptera | *Acyrthosiphon pisum* | pea aphid | ✓ | 42 | 52 | 3 | 5 |
| Arthropoda | Class Crustacea | *Daphnia pulex* | common water flea | ✓ | 39 | 52 | 3 | 5 |
| Arthropoda | Class Myriapoda | *Strigamia maritima* | littoral centipede | ✓ | 38 | 52 | 3 | 5 |
| Arthropoda | Class Arachnida / Parasitiformes | *Ixodes scapularis* | Blacklegged Tick | ✓ | 39 | 52 | 3 | 5 |
| Arthropoda | Class Arachnida / Acaraformes | *Tetranychus urticae* | spider mite | ✓ | 39 | 51 | 3 | 5 |
| Nematoda | Order Trichocephalida | *Trichinella spiralis* | parasitic roundworm | ✓ | 43 | 48 | 3 | 5 |
| Nematoda | Order Diplogastrida | *Pristionchus pacificus* | freee-living diplogastrid nematode | ✓ | 46 | 52 | 3 | 6 |
| Nematoda | Order Rhabditida | *Heterorhabditis bacteriophora* | entomopathogenic nematode | ✓ | 43 | 50 | 3 | 6 |
| Nematoda | Order Rhabditida | *Strongyloides ratti* | gastrointestinal parasitic nematode | ✓ | 43 | 52 | 3 | 5 |
| Nematoda | Order Rhabditida | *Caenorhabditis elegans* | free-living roundworm | ✓ | 43 | 50 | 3 | 5 |
| Nematoda | Order Rhabditida | *Caenorhabditis briggsae* | free-living roundworm | ✓ | 43 | 50 | 3 | 5 |
| Nematoda | Order Tylenchida | *Meloidogyne hapla* | Northern Root-Knot Nematode | ✓ | 43 | 50 | 3 | 5 |
| Nematoda | Order Tylenchida | *Bursaphelenchus xylophilus* | Pine Wilt Nematode | ✓ | 43 | 55 | 3 | 3 |
| Nematoda | Order Ascaridida | *Ascaris suum* | porcine parasitic roundworm | ✓ | 43 | 53 | 3 | 5 |
| Nematoda | Order Spirurida | *Loa loa* | African Eye Worm | ✓ | 42 | | 3 | |
| Nematoda | Order Spirurida | *Wuchereria bancrofti* | filarial nematode | ✓ | 42 | | 3 | |
| Nematoda | Order Spirurida | *Brugia malayi* | filarial nematode | ✓ | 42 | | 3 | |
| Platyhelminthes | Class Turbellaria | *Schmidtea mediterranea* | Freshwater Planarian | ✓ | 38 | | 3 | |
| **Non-vertebrate Bilateria (exon 12a = 38-46 aa, tri-cysteine motif; exon 12b = 48-55 aa, penta-cysteine motif)** | | | | **AVG** | **40.7** | **52.1** | **3.0** | **5.0** |
| sodium-permeant and sodium impermeant calcium channels | | | | **SE** | **0.4** | **0.4** | | |
| | | | | **RANGE** | **38-46** | **48-55** | | |
| Cnidaria | Class Anthozoa | *Nematostella vectensis* | Starlet sea anemone | | 39 | | 0 | |
| Cnidaria | Class Hydrozoa | *Acropora digitifera* | Table coral | | 39 | | 0 | |
| Cnidaria | Class Hydrozoa | *Hydra magnipapillata* | freshwater hydrozoan polyp | | 34 | | 0 | |
| Placozoa | Class Trichoplacia | *Trichoplax adhaerens* | placozoan | | 40 | | 2 | |
| **Basal metazoan (exon 12a = ~34-40 aa, 0-2 cysteines motif)** | | | | **AVG** | **38.0** | | **0.5** | |
| sodium-permeant calcium channels? | | | | **SE** | **1.4** | | **0.5** | |
| | | | | **RANGE** | **34-40** | | **0-2** | |

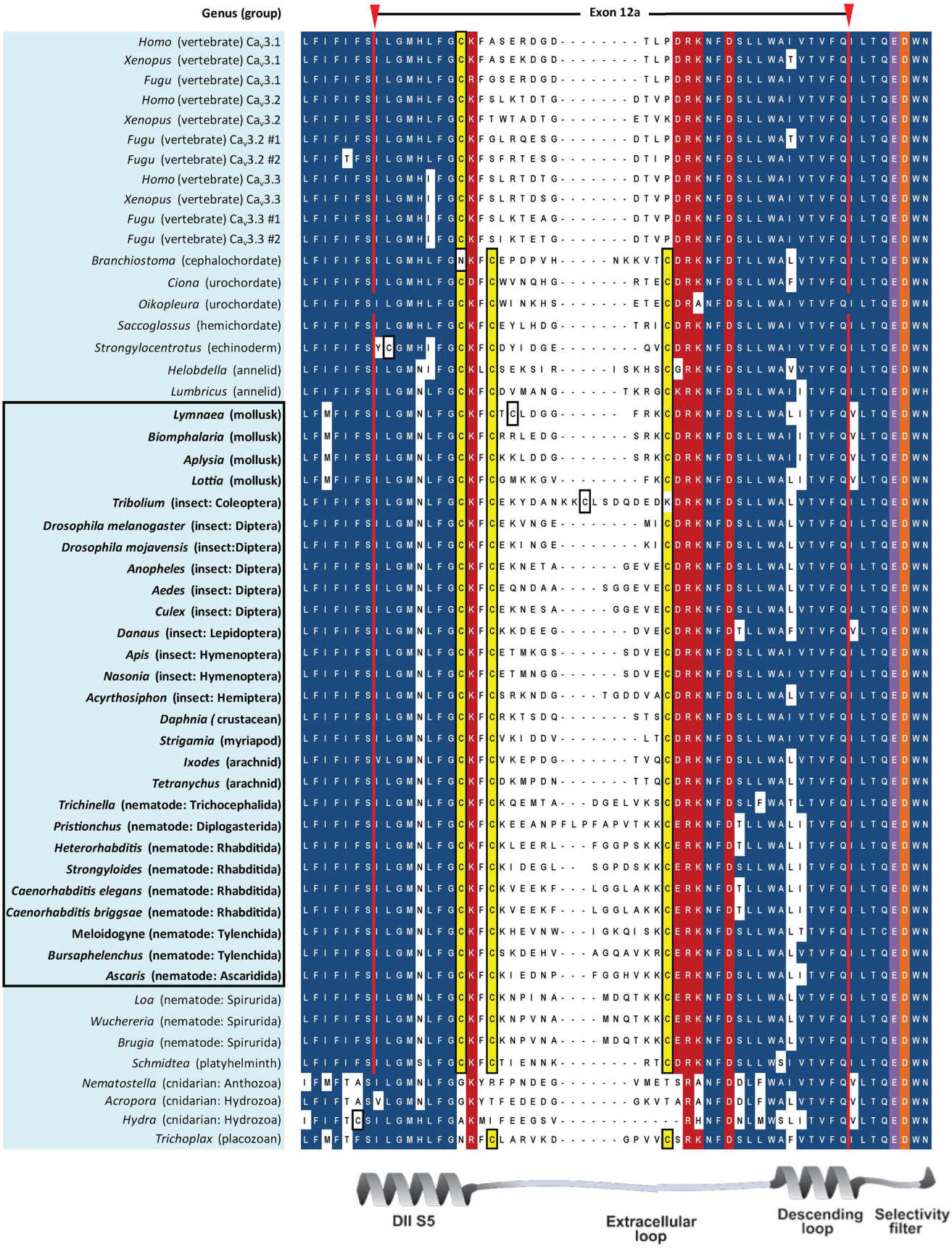
Genus (group)
Exon 12a
Homo (vertebrate) Cav3.1
Xenopus (vertebrate) Cav3.1
Fugu (vertebrate) Cav3.1
Homo (vertebrate) Cav3.2
Xenopus (vertebrate) Cav3.2
Fugu (vertebrate) Cav3.2 #1
Fugu (vertebrate) Cav3.2 #2
Homo (vertebrate) Cav3.3
Xenopus (vertebrate) Cav3.3
Fugu (vertebrate) Cav3.3 #1
Fugu (vertebrate) Cav3.3 #2
Branchiostoma (cephalochordate)
Ciona (urochordate)
Oikopleura (urochordate)
Saccoglossus (hemichordate)
Strongylocentrotus (echinoderm)
Helobdella (annelid)
Lumbricus (annelid)
Lymnaea (mollusk)
Biomphalaria (mollusk)
Aplysia (mollusk)
Lottia (mollusk)
Tribolium (insect: Coleoptera)
Drosophila melanogaster (insect: Diptera)
Drosophila mojavensis (insect:Diptera)
Anopheles (insect: Diptera)
Aedes (insect: Diptera)
Culex (insect: Diptera)
Danaus (insect: Lepidoptera)
Apis (insect: Hymenoptera)
Nasonia (insect: Hymenoptera)
Acyrthosiphon (insect: Hemiptera)
Daphnia ( crustacean)
Strigamia (myriapod)
Ixodes (arachnid)
Tetranychus (arachnid)
Trichinella (nematode: Trichocephalida)
Pristionchus (nematode: Diplogasterida)
Heterorhabditis (nematode: Rhabditida)
Strongyloides (nematode: Rhabditida)
Caenorhabditis elegans (nematode: Rhabditida)
Caenorhabditis briggsae (nematode: Rhabditida)
Meloidogyne (nematode: Tylenchida)
Bursaphelenchus (nematode: Tylenchida)
Ascaris (nematode: Ascaridida)
Loa (nematode: Spirurida)
Wuchereria (nematode: Spirurida)
Brugia (nematode: Spirurida)
Schmidtea (platyhelminth)
Nematostella (cnidarian: Anthozoa)
Acropora (cnidarian: Hydrozoa)
Hydra (cnidarian: Hydrozoa)
Trichoplax (placozoan)
DII S5
Extracellular loop
Descending loop
Selectivity filter

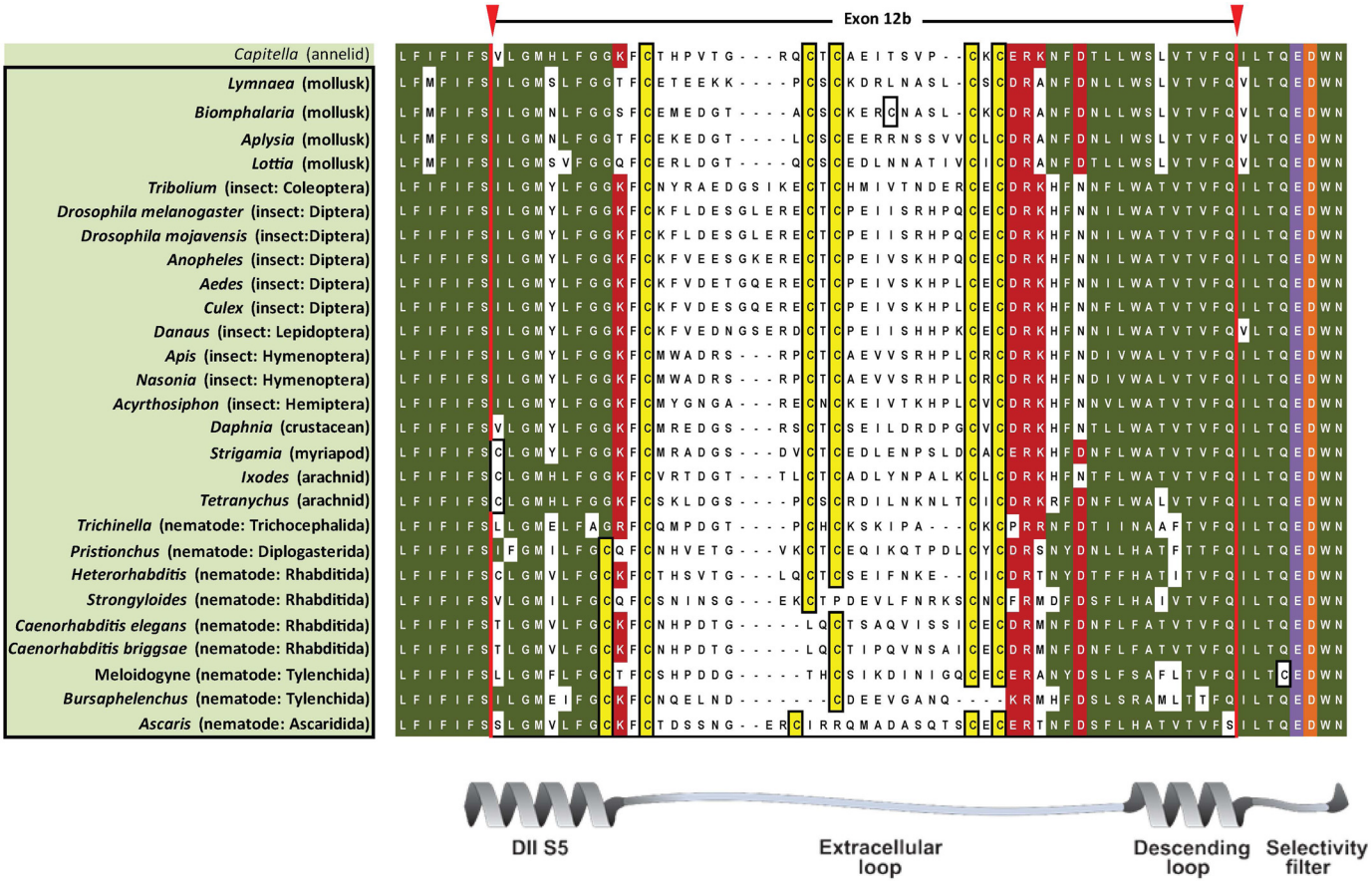


FIGURE 9. **Aligned amino acid sequences of exon 12B found in protostome $Ca_v3$ channel homologs.** Exons 12B code for novel extracellular turret residues from the middle of domain II, segment five through the descending pore helix to five amino acids upstream of selectivity filter glutamate (*purple*) residue, and invariant aspartate residue after it, conserved in all calcium channels (*orange residue*). 12b exons are flanked by conserved charged residues (*red*), surrounding a set of variable amino acids, outside of very conserved cysteine (*yellow*) residues. Exon 12b is ~52 aa with a penta-cysteine motif (C . . . *CXC* . . . *CXC*) or more rarely (*CXXC* . . . C . . *CXC*), in some nematodes. Most protostome invertebrates possess a shorter alternative exon 12a turret (see Fig. 8) in addition to longer exon 12b, and these are *highlighted* and *outlined*.

counterpart to the $Ca_v1$ and $Ca_v2$ calcium channels. We have isolated and characterized the singleton T-type channel, $TCa_v3$, cloned from the most primitive, extant relative to have a T-type channel, the placozoan *Trichoplax*, which is multicellular but lacks a tissue level organization. $TCa_v3$ generates calcium currents consistent with other basal metazoans, such as the hydrozoan jellyfish where it serves as the only calcium current generated in muscle action potentials (33). All basal metazoans have short exon 12 turrets with a small number of cysteines (0 to 2). Insertion of an intron before exon 12 in primitive protostomes, the platyzoa (acoelomates), allowed a duplication of exon 12 to generate dual turrets, one highly sodium-permeant tri-cysteine turret (exon 12a) and a more calcium-selective penta-cysteine turret (exon 12b) in ecdysozan and lophotrochozoan protostomes. Associated with protostomes is the appearance of the coelom and internal organs such as the heart, which require fast sodium-dependent spikes to coordinate the activities of their body organs. $Na_v1$ channels in vertebrates expanded to 10 $Na_v1$ channel genes fulfilling a universal spike generator role inside and outside the brain. Invertebrates, however, have a singleton $Na_v1$ sodium channel gene, which is absent in many species (*e.g. C. elegans*) and is not abundant outside the nervous system (*e.g. Lymnaea* snail). Outfitting sodium-permeant pores in T-type channels is a likely adaptation in invertebrates in lieu of spikes generated by $Na_v1$ channels.

*Importance of High Field Strength Site in Selectivity Filter Governing Calcium and Sodium Permeation*—Ion channels have evolved unique ion pores that are selective for the two major external cations, calcium ions and sodium ions. Flexible side chains of carboxylate oxygens from negatively charged residues are proposed to bind cations with high affinity, and permeation is facilitated by incoming ions attracted to the negatively charged extracellular surface of the pore (34). These

FIGURE 8. **Aligned amino acid sequences of exon 12A in metazoan $Ca_v3$ channel homologs.** Exon 12a codes for novel extracellular turret residues from the middle of domain II, segment five through the descending pore helix to five amino acids upstream of selectivity filter glutamate (*purple*) residue, and invariant aspartate residue after it, conserved in all calcium channels (*orange residue*). Exon 12a is flanked by conserved charged residues (*red*), surrounding a set of variable amino acids, outside of very conserved cysteine (*yellow*) residues. Exon 12a is ~40 aa with a tri-cysteine motif (*CXXC* . . . C). Vertebrate T-type channels resemble the size of exon 12A in length (~39 aa) but are missing the most downstream two cysteines of invertebrate exon 12a. Animals bearing T-type channels below the protostome invertebrates (placozoan and cnidarians) have zero or two cysteines in exon 12a and lack an exon 12b. Most protostome invertebrates possess an alternative exon 12b (see Fig. 9) turret in addition to exon 12a, and these are *highlighted* and *outlined*.

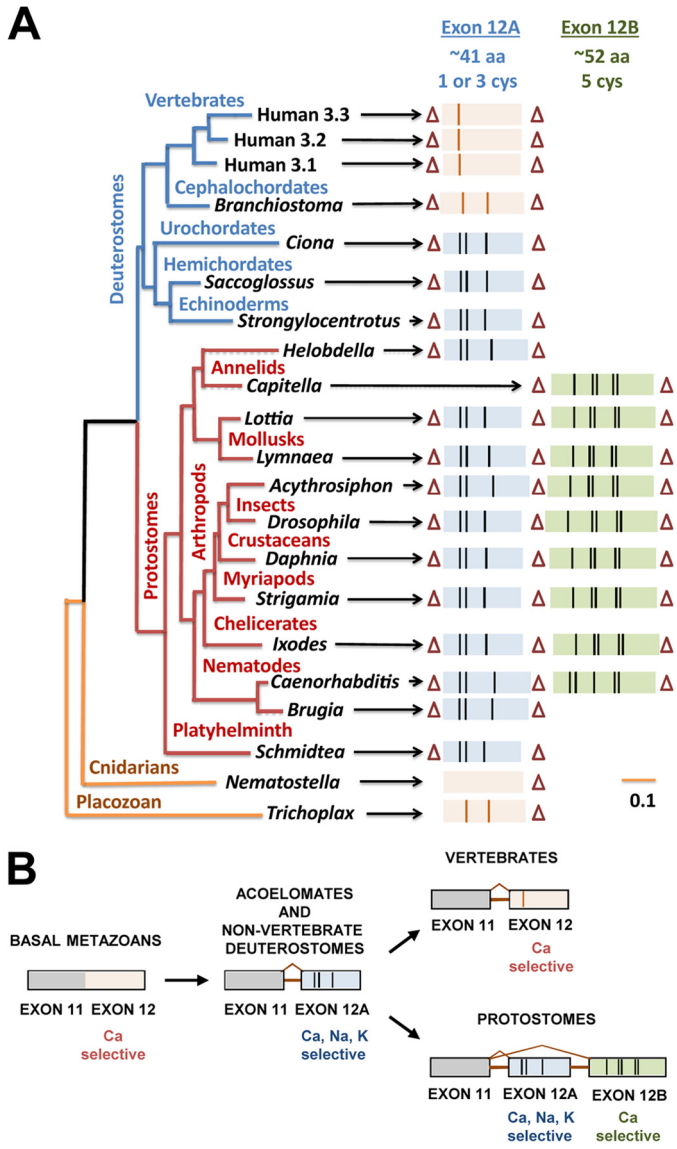


FIGURE 10. **Phylogeny and proposed evolution for exon 12, which governs monovalent ion permeability in $Ca_v3$ T-type channels.** *A,* gene tree illustrates the conservation of exon 12a (*smaller, blue exons*) and exon 12b (*larger, green exons*) with *vertical black lines* indicating location of cysteine residues. Introns are indicated by *triangles*. *B,* proposed evolutionary progression; an intron separating exons 11 and 12; appearance of a tri-cysteine motif characteristic of exon 12a highly sodium-permeant isoforms; an alternative exon 12b with a penta-cysteine motif characteristic of less sodium-permeant channels in protostomes. Evolution of a uni-cysteine motif in exon 12 of $Ca_v3$ channels that supports a more calcium-selective channel in vertebrates is shown.

charged residues form a "high field strength site" at the outer end of the selectivity filter in equivalent position of the selectivity filter TL**E**SWSM in the re-entrant pore contributed by equal domains of the homomultimeric prokaryotic sodium channel, NavAb (6). Backbone carbonyl residues of the preceding two residues **TL**ESWSM form the two innermost ion coordination sites for the sodium channel's selectivity filter (6). Replacement with three aspartates TL**DD**WS**D** in the selectivity filter transforms the sodium-selective pore into a calcium-selective one in prokaryotic channels (35, 36). Significantly, sodium and calcium ions enter, reside, and exit through the selectivity filter in a semi- or fully hydrated form through a much broader pore than a potassium-selective pore, and where strategic positioning of a limited number of residues can tip the balance in favor of whether mostly sodium or calcium ions or a mixture of both ions permeate (35). The sodium and calcium pore is a departure from the long and narrow potassium selectivity filter (TVGYG), which is a Goldilocks' "just right" fit for the dehydrated potassium ion, which underlies the potassium channels' nearly exclusive selectivity for potassium ions (5).

Identity of the single amino acid base of the equivalent field strength glutamate residue in prokaryotic sodium channels serves as the basis for categorizing metazoan sodium and calcium channels. This position is contributed by four nonequivalent residues of domains I–IV, in four domain-containing channels that contain a lysine in the domains III or II as DE**K**A (or D**K**EA) for Nav1 sodium-selective channels and lack a lysine residue in the calcium-selective $Ca_v1$ (EEEE), $Ca_v2$ (EEEE), and primordial $Na_v1$ (DEEA) or invertebrate $Na_v2$ channels, DEEA (37). The importance of this residue position is evident in experiments where sodium channels take on the high calcium selectivity of calcium channels after replacement of the DEKA high field strength site position with EEEE and vice versa (8, 38).

Yet it is clear that the high field strength site in the selectivity filter is not the only critical feature to govern permeation through T-type channels. All T-type channels have a unique high field strength site residue of EEDD, but when mutated to more resemble calcium-selective $Ca_v1$ and $Ca_v2$ channels (as EE**E**D or EED**E**), T-type channels become paradoxically more permeable and not less permeable to sodium ions (22). Despite the consistency in the EEDD high field strength site, T-type channels vary greatly in their sodium permeability that ranges from 20, 25, and 40% of the current for $Ca_v3.1$, $Ca_v3.2$, and $Ca_v3.3$ channels, respectively, for mammalian channels (1) and from 50 and >90% of the current through snail LCav3 channels with alternative novel extracellular S5-P turret regions in domain II. T-type channels also vary widely in their relative permeation of calcium ions as the charge carrier *versus* barium ions, which is expected to reflect a variable calcium affinity for the pores of T-type channels (10). This is in contrast to other calcium channels. Macroscopic barium currents are consistently ~2-fold the size of calcium currents, regardless of whether these are invertebrate Cav1 or Cav2 channels or vertebrate Cav1 or Cav2 homologs (1).

So, how do invertebrate T-type channels become so highly sodium-permeant using alternative splicing of extracellular regions outside the selectivity filter of the pore in domain II? Snail exons 12a and 12b differ in the extracellular turret, but there are also sequence differences that may be important in the descending helix just upstream of the selectivity filter in domain II. We suggest that changes in the descending helix and the extracellular turret could contribute to the altered sodium permeation through T-type channels.

*Potential Roles for Changes in the Descending Helix*—The distal end of the descending helix away from the selectivity filter has three variable amino acid residues as follows: AIV, ALI, and SLV in Cav3.1 and snail $LCa_v3$-12a and $LCa_v3$-12b channels, respectively. Negatively charged residues within the selectivity filter form transient binding partners outside the selectivity filter in structural intermediates of the calcium channel pore.

Changes in the descending helix may be sufficient to reorient a selectivity filter residue, altering the relative permeation of sodium and calcium ions.

*Potential Similarities of the T-type Channel Turret with the Extracellular Cap Domain of $K_{2P}$ Channels*—There are possibilities of analogy between the extracellular turret of domain II in T-type channels and the crystal structures of turret regions from two-pore potassium leak channels ($K_{2P}$) channels (40, 41).

The first of two pores of $K_{2P}$ channels has a uniquely extended turret of 56 amino acids, which normally ranges between 5 and 20 amino acids in other potassium channels. The turret forms a highly ordered extracellular cap, reminiscent of an A-frame, extending 35 Å above the lipid membrane with a cysteine residue at its apex, which cross-links to the apex of the A-frame of a second $K_{2P}$ subunit, in the 2-fold symmetrical $K_{2P}$ channel (40, 41). The dual A-frames perpendicular to each other form a space-filled "carafe plug" that restricts ion and drug access to the channel pore from above (40, 41). $K^+$ ion passage is limited to two funnel-shaped side portals contained in the extracellular cap domain (40, 41). Walls along the side portals are lined with negatively charged residues and variable sequences that could serve as a variable pre-filter for cations channeling to the selectivity filter below (40, 41). The extracellular cap domain approaches close to the selectivity filter where the negative C-terminal ends of the helical dipole from an extracellular helix lie just above and to the side of the selectivity filter, before sharply pivoting away from the selectivity filter at a conserved glycine residue before meeting with the descending pore helix that leads to the selectivity filter (40, 41).

The turret in domain II of T-type channels is the shortest of the four extracellular turrets preceding the pore helices that descend into the re-entrant pore and thus is likely restricted to the lower quadrant of the outer vestibule where it may likely encounter the selectivity filter (1). The constraints on size and the conserved framework of uni-, tri-, and penta-cysteine exon 12 in vertebrates and exons 12a and 12b of invertebrate T-type channels are consistent with these specialized turret variants changing the landscape in the external vestibule (analogously to $K_{2P}$ channels) and forming regulatory structures that make specific contacts within the pore. Differing turrets are expected to bias the selectivity filter allowing the more favored passage of monovalent over divalent cations in a pore that is expected to be similar to the wide bacterial sodium channel (*e.g.* $Na_vAb$ (6) and $Na_vRh$ (42)), which can accommodate more than one semi-hydrated ion at its more constrictive locus (the selectivity filter residues).

*Possible Similarity of the Extracellular Turret Domains in $K_{2P}$, $K_{IR}$, and T-type Channels as Toxin Defense Shields*—Eukaryotic inward-rectifying potassium channels ($K_{IR}$) also possess an extended turret region, albeit a minor external appendage compared with $K_{2P}$ channels (43). Nonetheless, the turret of $K_{IR}$ channels is substantial enough to alter the external surface landscape and to contribute a unique resistance of these channels to classical invertebrate toxins (*e.g.* from snake, spider, and scorpion venom), which typically block voltage-gated potassium channels when applied from the outside of the channels (44–46). Resistance to external toxins is a shared property with $K_{2P}$ channels likely due to shielding with the elaborate extracellular cap domain of $K_{2P}$ channels (47, 48). Unique extracellular turret domains may also explain why there are not invertebrate pore-blocking toxins (from cone snail, spider, and snake venom) for $Ca_v3$ T-type channels compared with other ($Ca_v1$ and $Ca_v2$) calcium channels, where numbers of specific high affinity toxins have been discovered (49). The extensive extracellular turret regions in $K_{2P}$ (40, 41), eukaryotic $K_{IR}$ (43), and T-type channels are highly variable in sequence outside of key structural residues (*e.g.* cysteines, glycine, and prolines) or in the positioning of particular charged residues (*e.g.* arginine and lysine). One can imagine that some sequence variation in extracellular regions may be adaptive as counter-measures against the arsenal of specific channel toxins from the venom of invertebrate predators.

*Other Examples of Alternative Splicing That Generates Altered Ion Selectivity of Ion Channels*—Alternative splicing that generates permeation differences in ion channels is not common. We discovered alternative exons in domain II of NALCN channels that alter the high field strength residue to generate calcium-like (EEEE) or sodium-like (E**K**EE) pores (of flatworms, mollusks, annelids, echinoderms, and hemichordates) (19, 50). Interestingly, some arthropods generate alternative pores in NALCN channels differently, using an alternative exon in domain III to generate calcium-like (EEEE) or sodium-like (EE**K**E) pores in their NALCN channels (19, 50). Finally, a completely unique approach to altering ion selectivity is the use of alternative translational start sites to generate a truncated isoform in $K_{2P}2.1$ channels that are sodium-permeable, to produce offsetting depolarizing currents in a channel type that typically only serves up hyperpolarizing potassium leak currents (39).

*Conclusions*—T-type channels have varying sodium permeability in the presence of an extracellular veil of novel turret residues in domain II, which encode merely ~1% of the T-type channel protein. Each splice isoform is exclusively expressed in particular tissues, where they serve highly different functions conducting variable sodium and calcium currents. It is surprising that only a few amino acids separate highly sodium- or more calcium-conducting channels, given that the ions have such different roles, where $Na^+$ ions are relatively inert and are much more abundant serving mostly an electrogenic role, and $Ca^{2+}$ ions are maintained at very low levels in cells due to cytotoxicity, and serve as an exquisitely sensitive signaling molecule. Extracellular concentrations of sodium ions are on the scale of approximately fifty times that of $Ca^{2+}$ ions or $K^+$ ions, so T-type channels that are permeant to monovalent ions are generating large currents and steeper membrane depolarizations than typical calcium-selective channels. They also generate larger currents than high voltage-activated calcium channels because of the greater driving force for T-type channels operating at their much lower voltage range.

It is remarkable that T-type channels evolved a mechanism outside the conventional selectivity filter to alter their ion selectivity. It is also intriguing to understand the physiological context (*e.g.* for brain, heart and glands) in which T-type channels retain similar biophysical properties but possess dramatically different ion selectivities for sodium and calcium ions.

*Acknowledgments—We are grateful to Wic Wildering and Petra Hermann for their generous shipments of L. stagnalis* to complete this work and Martin Rioux for assistance in generating preliminary materials for the project.

## REFERENCES


1. Senatore, A., Guan, W., and Spafford, J. D. (2014) Cav3 T-type channels: Regulators for its gating, membrane expression and cation selectivity. *Pflugers Arch.* **466,** 645–660
2. Senatore, A., Monteil, A., van Minnen, J., Smit, A. B., and Spafford, J. D. (2013) NALCN ion channels have alternative selectivity filters resembling calcium channels or sodium channels. *PLoS One* **8,** e55088
3. Senatore, A., Zhorov, B. S., and Spafford, J. D. (2012) $Ca_V3$ T-type calcium channels. *WIREs Membr. Transp. Signal.* **1,** 467–491
4. Strong, M., Chandy, K. G., and Gutman, G. A. (1993) Molecular evolution of voltage-sensitive ion channel genes: On the origins of electrical excitability. *Mol. Biol. Evol.* **10,** 221–242
5. Doyle, D. A., Morais Cabral, J., Pfuetzner, R. A., Kuo, A., Gulbis, J. M., Cohen, S. L., Chait, B. T., and MacKinnon, R. (1998) The structure of the potassium channel: Molecular basis of $K^+$ conduction and selectivity. *Science* **280,** 69–77
6. Payandeh, J., Scheuer, T., Zheng, N., and Catterall, W. A. (2011) The crystal structure of a voltage-gated sodium channel. *Nature* **475,** 353–358
7. McCusker, E. C., Bagnéris, C., Naylor, C. E., Cole, A. R., D'Avanzo, N., Nichols, C. G., and Wallace, B. A. (2012) Structure of a bacterial voltage-gated sodium channel pore reveals mechanisms of opening and closing. *Nat. Commun.* **3,** 1102
8. Heinemann, S. H., Terlau, H., Stühmer, W., Imoto, K., and Numa, S. (1992) Calcium channel characteristics conferred on the sodium channel by single mutations. *Nature* **356,** 441–443
9. Hess, P., Lansman, J. B., and Tsien, R. W. (1986) Calcium channel selectivity for divalent and monovalent cations. Voltage and concentration dependence of single channel current in ventricular heart cells. *J. Gen. Physiol.* **88,** 293–319
10. Shcheglovitov, A., Kostyuk, P., and Shuba, Y. (2007) Selectivity signatures of three isoforms of recombinant T-type $Ca^{2+}$ channels. *Biochim. Biophys. Acta* **1768,** 1406–1419
11. Khan, N., Gray, I. P., Obejero-Paz, C. A., and Jones, S. W. (2008) Permeation and gating in CaV3.1 ($\alpha$1G) T-type calcium channels effects of $Ca^{2+}$, $Ba^{2+}$, $Mg^{2+}$, and $Na^+$. *J. Gen. Physiol.* **132,** 223–238
12. Kostyuk, P. G., Mironov, S. L., and Shuba, Y. M. (1983) Two ion-selecting filters in the calcium channel of the somatic membrane of mollusc neurons. *J. Membr. Biol.* **76,** 83–93
13. Senatore, A., and Spafford, J. D. (2010) Transient and big are key features of an invertebrate T-type channel (LCav3) from the central nervous system of *Lymnaea stagnalis*. *J. Biol. Chem.* **285,** 7447–7458
14. Senatore, A., and Spafford, J. D. (2012) Gene transcription and splicing of T-type channels are evolutionarily conserved strategies for regulating channel expression and gating. *PLoS One* **7,** e37409
15. Yeoman, M. S., Brezden, B. L., and Benjamin, P. R. (1999) LVA and HVA $Ca^{2+}$ currents in ventricular muscle cells of the *Lymnaea* heart. *J. Neurophysiol.* **82,** 2428–2440
16. Brezden, B. L., Yeoman, M. S., Gardner, D. R., and Benjamin, P. R. (1999) FMRFamide-activated $Ca^{2+}$ channels in *Lymnaea* heart cells are modulated by "SEEPLY," a neuropeptide encoded on the same gene. *J. Neurophysiol.* **81,** 1818–1826
17. Senatore, A., Boone, A. N., and Spafford, J. D. (2011) Optimized transfection strategy for expression and electrophysiological recording of recombinant voltage-gated ion channels in HEK-293T cells. *J. Vis. Exp.* **19,** 2314
18. Hille, B. (2001) *Ion Channels of Excitable Membranes,* 3rd Ed., pp. 441–470, Sinauer Associates, Inc., Sunderland, MA
19. Senatore, A., Monteil, A., van Minnen, J., Smit, A. B., and Spafford, J. D. (2013) NALCN ion channels have alternative selectivity filters resembling calcium channels or sodium channels. *PLoS One* **8,** e55088
20. Dawson, T. F., Boone, A. N., Senatore, A., Piticaru, J., Thiyagalingam, S., Jackson, D., Davison, A., and Spafford, J. D. (2014) Gene splicing of an invertebrate $\beta$ subunit (LCav$\beta$) in the N-terminal and HOOK domains and its regulation of LCav1 and LCav2 calcium channels. *PLoS One,* in press
21. McComb, C., Varshney, N., and Lukowiak, K. (2005) Juvenile *Lymnaea* ventilate, learn and remember differently than do adult *Lymnaea*. *J. Exp. Biol.* **208,** 1459–1467
22. Talavera, K., Staes, M., Janssens, A., Klugbauer, N., Droogmans, G., Hofmann, F., and Nilius, B. (2001) Aspartate residues of the Glu-Glu-Asp-Asp (EEDD) pore locus control selectivity and permeation of the T-type $Ca^{2+}$ channel $\alpha$(1G). *J. Biol. Chem.* **276,** 45628–45635
23. Eisenman, G., Sandblom, J. P., and Walker, J. L., Jr. (1967) Membrane structure and ion permeation. Study of ion exchange membrane structure and function is relevant to analysis of biological ion permeation. *Science* **155,** 965–974
24. Senatore, A., Boone, A., Lam, S., Dawson, T. F., Zhorov, B., and Spafford, J. D. (2011) Mapping of dihydropyridine binding residues in a less sensitive invertebrate L-type calcium channel (LCa v 1). *Channels* **5,** 173–187
25. Huang, X., Senatore, A., Dawson, T. F., Quan, Q., and Spafford, J. D. (2010) G-proteins modulate invertebrate synaptic calcium channel (LCa(v)2) differently from the classical voltage-dependent regulation of mammalian Ca(v)2.1 and Ca(v)2.2 channels. *J. Exp. Biol.* **213,** 2094–2103
26. Ono, K., and Iijima, T. (2005) Pathophysiological significance of T-type $Ca^{2+}$ channels: properties and functional roles of T-type $Ca^{2+}$ channels in cardiac pacemaking. *J. Pharmacol. Sci.* **99,** 197–204
27. Nagle, G. T., de Jong-Brink, M., Painter, S. D., and Li, K. W. (2001) Structure, localization and potential role of a novel molluscan trypsin inhibitor in *Lymnaea*. *Eur. J. Biochem.* **268,** 1213–1221
28. Nikitin, E. S., Vavoulis, D. V., Kemenes, I., Marra, V., Pirger, Z., Michel, M., Feng, J., O'Shea, M., Benjamin, P. R., and Kemenes, G. (2008) Persistent sodium current is a nonsynaptic substrate for long-term associative memory. *Curr. Biol.* **18,** 1221–1226
29. Opdyke, C. A., and Calabrese, R. L. (1994) A persistent sodium current contributes to oscillatory activity in heart interneurons of the medicinal leech. *J. Comp. Physiol. A* **175,** 781–789
30. Hodgkin, A. L., and Katz, B. (1949) The effect of sodium ions on the electrical activity of giant axon of the squid. *J. Physiol.* **108,** 37–77
31. Hobert, O. (2013) The neuronal genome of *Caenorhabditis elegans*. *WormBook*, 2013, 1–106
32. Biel, M., Wahl-Schott, C., Michalakis, S., and Zong, X. (2009) Hyperpolarization-activated cation channels: From genes to function. *Physiol. Rev.* **89,** 847–885
33. Lin, Y. C., and Spencer, A. N. (2001) Calcium currents from jellyfish striated muscle cells: Preservation of phenotype, characterisation of currents and channel localisation. *J. Exp. Biol.* **204,** 3717–3726
34. Cheng, R. C., Tikhonov, D. B., and Zhorov, B. S. (2010) Structural modeling of calcium binding in the selectivity filter of the L-type calcium channel. *Eur. Biophys. J.* **39,** 839–853
35. Tang, L., Gamal El-Din, T. M., Payandeh, J., Martinez, G. Q., Heard, T. M., Scheuer, T., Zheng, N., and Catterall, W. A. (2014) Structural basis for $Ca^{2+}$ selectivity of a voltage-gated calcium channel. *Nature* **505,** 56–61
36. Yue, L., Navarro, B., Ren, D., Ramos, A., and Clapham, D. E. (2002) The cation selectivity filter of the bacterial sodium channel, NaChBac. *J. Gen. Physiol.* **120,** 845–853
37. Liebeskind, B. J., Hillis, D. M., and Zakon, H. H. (2011) Evolution of sodium channels predates the origin of nervous systems in animals. *Proc. Natl. Acad. Sci. U.S.A.* **108,** 9154–9159
38. Schlief, T., Schönherr, R., Imoto, K., and Heinemann, S. H. (1996) Pore properties of rat brain II sodium channels mutated in the selectivity filter domain. *Eur. Biophys. J.* **25,** 75–91
39. Thomas, D., Plant, L. D., Wilkens, C. M., McCrossan, Z. A., and Goldstein, S. A. (2008) Alternative translation initiation in rat brain yields K2P2.1 potassium channels permeable to sodium. *Neuron* **58,** 859–870
40. Brohawn, S. G., del Mármol, J., and MacKinnon, R. (2012) Crystal structure of the human K2P TRAAK, a lipid- and mechano-sensitive $K^+$ ion channel. *Science* **335,** 436–441
41. Miller, A. N., and Long, S. B. (2012) Crystal structure of the human two-pore domain potassium channel K2P1. *Science* **335,** 432–436
42. Zhang, X., Ren, W., DeCaen, P., Yan, C., Tao, X., Tang, L., Wang, J.,

Hasegawa, K., Kumasaka, T., He, J., Wang, J., Clapham, D. E., and Yan, N. (2012) Crystal structure of an orthologue of the NaChBac voltage-gated sodium channel. *Nature* **486,** 130–134

43. Tao, X., Avalos, J. L., Chen, J., and MacKinnon, R. (2009) Crystal structure of the eukaryotic strong inward-rectifier $K^+$ channel Kir2.2 at 3.1 Å resolution. *Science* **326,** 1668–1674
44. Imredy, J. P., Chen, C., and MacKinnon, R. (1998) A snake toxin inhibitor of inward rectifier potassium channel ROMK1. *Biochemistry* **37,** 14867–14874
45. Jin, W., and Lu, Z. (1998) A novel high-affinity inhibitor for inward-rectifier $K^+$ channels. *Biochemistry* **37,** 13291–13299
46. Lu, Z., and MacKinnon, R. (1997) Purification, characterization, and synthesis of an inward-rectifier $K^+$ channel inhibitor from scorpion venom. *Biochemistry* **36,** 6936–6940
47. Fink, M., Lesage, F., Duprat, F., Heurteaux, C., Reyes, R., Fosset, M., and Lazdunski, M. (1998) A neuronal two P domain $K^+$ channel stimulated by arachidonic acid and polyunsaturated fatty acids. *EMBO J.* **17,** 3297–3308
48. Lesage, F., Guillemare, E., Fink, M., Duprat, F., Lazdunski, M., Romey, G., and Barhanin, J. (1996) TWIK-1, a ubiquitous human weakly inward rectifying $K^+$ channel with a novel structure. *EMBO J.* **15,** 1004–1011
49. Doering, C. J., and Zamponi, G. W. (2003) Molecular pharmacology of high voltage-activated calcium channels. *J. Bioenerg. Biomembr.* **35,** 491–505
50. Senatore, A., and Spafford, J. D. (2013) A uniquely adaptable pore is consistent with NALCN being an ion sensor. *Channels* **7,** 60–68